# Discovery of a Novel Class of Exquisitely Selective Mesenchymal-Epithelial Transition Factor (c-MET) Protein Kinase Inhibitors and Identification of the Clinical Candidate 2-(4-(1-(Quinolin-6-ylmethyl)-1H-[1,2,3]triazolo[4,5-b]pyrazin-6-yl)-1H-pyrazol-1-yl)ethanol (PF-04217903) for the Treatment of Cancer

J. Jean Cui,* Michele McTigue, Mitchell Nambu, Michelle Tran-Dubé, Mason Pairish, Hong Shen, Lei Jia, Hengmiao Cheng, Jacqui Hoffman, Phuong Le, Mehran Jalaie, Gilles H. Goetz,[§] Kevin Ryan, Neil Grodsky, Ya-li Deng, Max Parker, Sergei Timofeevski, Brion W. Murray, Shinji Yamazaki, Shirley Aguirre, Qiuhua Li, Helen Zou, and James Christensen

La Jolla Laboratories, Pfizer Worldwide Research and Development, 10770 Science Center Drive, San Diego, California 92121, United States

Ⓢ *Supporting Information*

ABSTRACT: The c-MET receptor tyrosine kinase is an attractive oncology target because of its critical role in human oncogenesis and tumor progression. An oxindole hydrazide hit **6** was identified during a c-MET HTS campaign and subsequently demonstrated to have an unusual degree of selectivity against a broad array of other kinases. The cocrystal structure of the related oxindole hydrazide c-MET inhibitor **10** with a nonphosphorylated c-MET kinase domain revealed a unique binding mode associated with the exquisite selectivity profile. The chemically labile oxindole hydrazide scaffold was

6, HTS Hit
c-Met Ki 0.101 μM
c-Met cell IC$_{50}$ >20 μM

2, PF-04217903
c-Met Ki 0.004 μM
c-Met cell IC$_{50}$ 0.005 μM
Exquisitely selective over 208 kinases

replaced with a chemically and metabolically stable triazolopyrazine scaffold using structure based drug design. Medicinal chemistry lead optimization produced 2-(4-(1-(quinolin-6-ylmethyl)-1H-[1,2,3]triazolo[4,5-b]pyrazin-6-yl)-1H-pyrazol-1-yl)-ethanol (**2**, **PF-04217903**), an extremely potent and exquisitely selective c-MET inhibitor. **2** demonstrated effective tumor growth inhibition in c-MET dependent tumor models with good oral PK properties and an acceptable safety profile in preclinical studies. **2** progressed to clinical evaluation in a Phase I oncology setting.
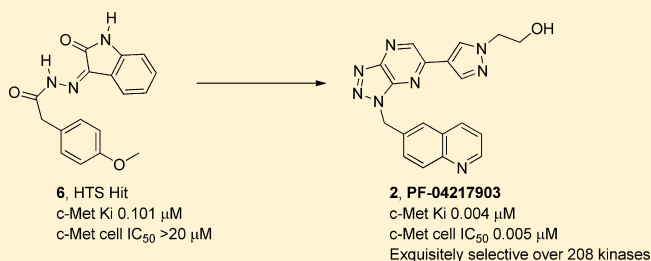
INTRODUCTION

c-MET, also called hepatocyte growth factor receptor (HGFR), belongs to a structurally unique subfamily of receptor tyrosine kinase (RTK), along with RON protein kinase. The natural ligand for c-MET is hepatocyte growth factor (HGF), also known as scatter factor. The c-MET/HGF signaling pathway plays important roles during normal development, organogenesis, and homeostasis. After activation by HGF, c-MET induces an invasive program consisting of cell proliferation, migration, invasion, and survival that is essential during normal processes, such as morphogenesis and wound healing.[1] Aberrant c-MET/HGF signaling through constitutive activation, gene amplification, mutations, and activation of an autocrine loop occurs in virtually all types of solid tumors, and as such is implicated in multiple tumor oncogenic processes, such as mitogenesis, survival, angiogenesis, and invasive growth, and especially in the metastatic process.[2] Furthermore, overexpression of c-MET and HGF was demonstrated to correlate with poor prognosis or metastatic progression in a number of major human cancers.[3] For these

reasons, c-MET and its ligand HGF are emerging as attractive targets for targeted cancer therapies.

The strategies to regulate the c-MET/HGF pathway include HGF antagonists (NK2 and NK4),[4] anti-HGF antibodies,[5] anti-c-MET monoclonal antibodies,[6] and c-MET small molecule inhibitors.[7] The anti-HGF antibody AMG 102 (rilotumumab), when combined with the anti-EGFR antibody panitumumab, showed a higher overall response rate for colorectal cancer patients than patients treated with panitumumab plus placebo in a randomized phase II study.[8] A durable, complete response of metastatic gastric cancer with high c-MET gene polysomy and evidence for an autocrine production of hepatocyte growth factor was achieved with c-MET monoclonal antibody MetMab.[9] Overexpression of c-MET in non-small-cell lung cancer (NSCLC) represents more than half of the population and is associated with a worse outcome. MetMab, in combination with erlotinib, significantly improved PFS and

OS, resulting in a near 3-fold reduction in the risk of death.[10] The first crystal structures of c-MET were published in 2002[11a] and 2003,[11b] which facilitate small molecule c-MET inhibitor development. Several classes of small molecule c-MET inhibitors with different binding modes and selectivity profiles progressed to clinical trials (Chart 1). Foretinib, a type II

Chart 1. Representative c-MET Inhibitors in Clinical Development

XL-880, foretinib

1, MK-2461

crizotinib

2, PF-04217903

ARQ-197, tivantinib
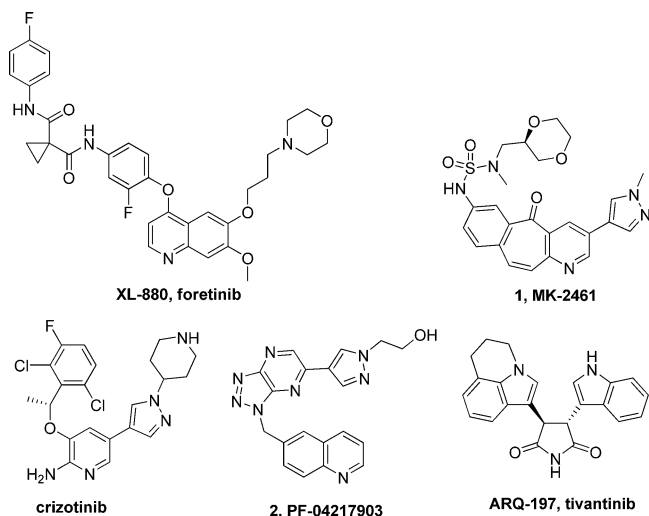
inhibitor bound into the deep hydrophobic back pocket, is a multitargeted c-MET/VEGFR2 inhibitor[12] and demonstrated partial regression or stable disease in patients with papillary renal carcinoma[13] and poorly differentiated gastric cancer.[14] MK-2461 (1) is a potent c-MET inhibitor that is selective for the inhibition of the phosphorylated c-MET enzyme.[15] 1 is currently in phase I/II clinic trials for cancer treatments. Crizotinib is a potent c-MET/ALK dual inhibitor[16] which demonstrated marked efficacy for a subset of NSCLC patients with an EML4-ALK fusion gene, leading to a fast track FDA approval.[17] In addition, crizotinib demonstrated a rapid and durable response for a NSCLC patient with *de novo MET* amplification, but without ALK rearrangement.[18] Patients with *MET*-amplified esophagogastric adenocarcinoma and glioblastoma achieved dramatic clinical improvement and radiographic regression upon treatment with crizotinib.[19,20] Tivantinib (ARQ-197) is reported as a non-ATP-competitive small molecule c-MET inhibitor;[21] albeit, it is bound at the ATP

binding site. When given with the EGFR inhibitor erlotinib in patients with NSCLC who have had prior chemotherapy but are EGFR TKI naïve, tivantinib may prolong PFS, extend OS, and delay metastases compared with treatment with erlotinib alone.[22] Strong interest in targets that inhibit the HGF/c-MET pathway is fueled by the continually emerging evidence of clinical benefit in a variety of cancers.

2-(4-(1-(Quinolin-6-ylmethyl)-1*H*-[1,2,3]triazolo[4,5-*b*]-pyrazin-6-yl)-1*H*-pyrazol-1-yl)ethanol (**2**, **PF-04217903**) is a potent and exquisitely selective ATP competitive c-MET inhibitor.[23] **2** demonstrated low nanomolar potency against c-MET in both *in vitro* cell assays and *in vivo* target modulation studies, and it showed effective tumor growth inhibition with good oral PK properties. **2** progressed to human clinical studies for oncology. Herein, we report the discovery of a unique c-MET autoinhibitory conformation and the medicinal chemistry effort which led to the discovery of the potent and exquisitely selective c-MET inhibitor **2**.

■ RESULTS AND DISCUSSION

Structural Elucidation of an HTS Hit. High throughput screening (HTS) is a powerful method for the identification of novel chemical series for a new target. The screening results for novel and efficient hits are highly dependent on the quality and diversification of the compound collection. Hundreds of thousands of compounds with diversified structural features were screened using an enzymatic assay that assessed c-MET inhibition. Compound **3** from the HTS campaign was an attractive hit with a K_i of 101 nM as an ATP competitive c-MET inhibitor. The structure of **3** was drawn according to the original compound database record (Chart 2). As a standard procedure for an HTS triage, attractive hits were subjected to analytical tests including LC-MS and NMR spectroscopy methods to confirm the compound identity. The active samples were also subjected to a process referred to as LC-MS-BA (liquid chromatography—mass spectrometry—bioassay), which simultaneously allowed for the assessments of sample purity and structure confirmation through generation of UV and mass spectra. The fraction from the chromatographic step in this process was collected for bioassay, and the comparisons between the chromatographic and bioassay profiles were made to determine whether the activity corresponded to the desired chromatographic peak. Using the LC-MS-BA method, it was discovered that the molecular weight of the active component of **3** (>90%) was 309.32, which was consistent with the structure of **4**. ^{1}H NMR of the active component
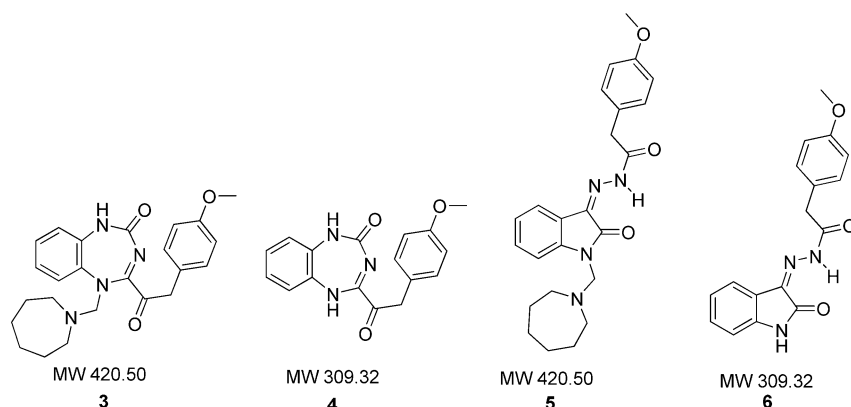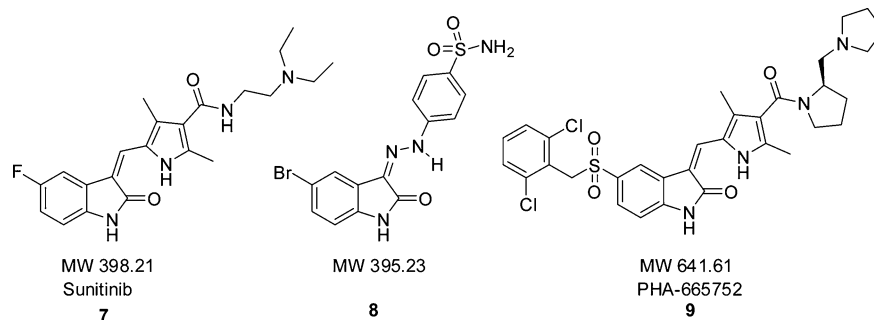
Chart 2. Structural Elucidation of an HTS Hit

MW 420.50
3

MW 309.32
4

MW 420.50
5

MW 309.32
6

Chart 3. Structures of Oxindole-Based Kinase Inhibitors

MW 398.21
Sunitinib
7

8

MW 641.61
PHA-665752
9

indicated the absence of the azepan-1-ylmethylene group, which further supported the proposal of the structure of **4**. A small molecule X-ray structure revealed that the real structure of **3** was actually the structure of **5**, a starting material used for the preparation of compound **3** with the same molecular formula and weight. As a result, the real structure of the active component was deduced to be the structure of **6**. **6** was synthesized and confirmed to have the same ^{1}H NMR and biological activity against c-MET as the active ingredient from the HTS. Thus, the highly efficient c-MET hit of **6** was successfully identified through careful structural elucidation of an HTS hit.

Discovery of an Exquisitely Selective c-MET Binding Mode. **6** is an attractive hit with high biochemical ligand efficiency (LE = $-RT \log K_i$/the number of heavy atoms = 0.42) and lipophilic efficiency (lipE = $-\log K_i - \text{cLogD} = 4.80$) against c-MET. In addition, **6** was highly selective for c-MET, showing an IC_{50} of >20 μM against a panel of other tyrosine and serine/threonine kinases (VEGFR2, EGFR, SRC, DDR, PDGFR, ZC1, PAK4, LCK, and LYN). Although the chemical instability of the hydrazide linkage has a potential safety liability associated with a possible release of the toxic hydrazine, the intriguing selectivity profile prompted further exploration of this hit. Oxindole-based chemical scaffolds have been broadly used as protein kinase inhibitors, with the oxindole generally making hydrogen bonds to the backbone of the kinase hinge segment in the active site of the kinase catalytic domain. Examples include sunitinib (**7**), a potent split kinase inhibitor,[24] and 3-hydrazono-1,3-dihydro-indol-2-one **8** as CDK2 inhibitor[25] (Chart 3). Based on the cocrystal structure of **8** with CDK2 (Figure 1a), it was rationalized that **6** should bind to c-MET with the oxindole hydrogen bonding to the kinase hinge, as occurs for most studied oxindole kinase inhibitors, and with the hydrazide extending out to the protein solvent area (Figure 1b).

Even though **7** is a potent inhibitor against split kinases including VEGFRs, PDGFR, and c-KIT, it is a relatively weak inhibitor against c-MET with an enzymatic IC_{50} of 5 μM. A dramatic increase in c-MET inhibitory potency was achieved with the introduction of a 5-benzylsulfonyl group on the 3-[1-(1H-pyrrol-2-yl)meth-(Z)-ylidene]-1,3-dihydroindol-2-one scaffold, as illustrated with PHA-665752 (**9**), a potent and selective c-MET inhibitor with a K_i of 9 nM.[26] The cocrystal structure of **9** with c-MET revealed a strong interaction of the 2,6-dichlorophenyl group with Tyr-1230,[16,27] which is critical for c-MET inhibition. A structural analysis was used to generate hypotheses for the molecular underpinnings of the inhibitory potency and kinase selectivity of **6**. The solvent exposure area is not expected to provide a high degree of kinase selectivity due
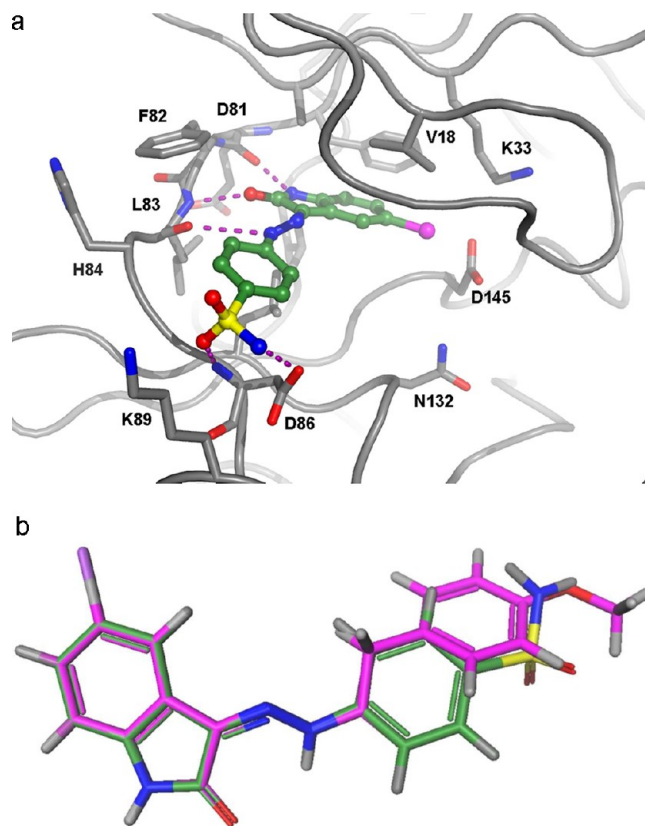

Figure 1. (a) Compound **8** bound in CDK2 (PDB ID 1FVT).[25] (b) Overlay of **8** with the proposed binding orientation of **6**.

to the flexibility and common structural features in this area. Moreover, the traditional oxindole binding mode would hardly rationalize the high ligand efficiency and selectivity of **6** against c-MET (Figure 1b). It was therefore predicated that **6** have a unique binding mode to c-MET for a profile with high ligand efficiency and selectivity. Chemistry optimization of **6** was carried out to gain further insight on the potential of the series. Demethylation of **6** improved potency dramatically, and the optimization of the substituents on the oxindole ring afforded analogs with improved enzymatic and cellular potencies, as illustrated with compound **10** having an enzymatic K_i of 1.3 nM and an IC_{50} of 7 nM for the inhibition of c-MET autophosphorylation in the A549 cell line.[28] Inhibition of phosphorylated c-MET KD in purified enzyme biochemical assays confirmed that the inhibitors can inhibit the active c-MET, and the cell-based activity of the inhibitors prevented RTK autophosphorylation, consistent with inhibitory interaction with the nonphosphorylated form in cells. The minor

divergence between the enzyme and cell activities of **10** implied the inhibition of both active and unactive c-MET.

A kinase domain (KD) construct of c-MET, in its nonphosphorylated form, was prepared for utilization in cocrystallization experiments. Indeed, the cocrystal structure of **10** with nonphosphorylated c-MET protein demonstrated a unique binding mode (Figure 2). Surprisingly, the oxindole ring
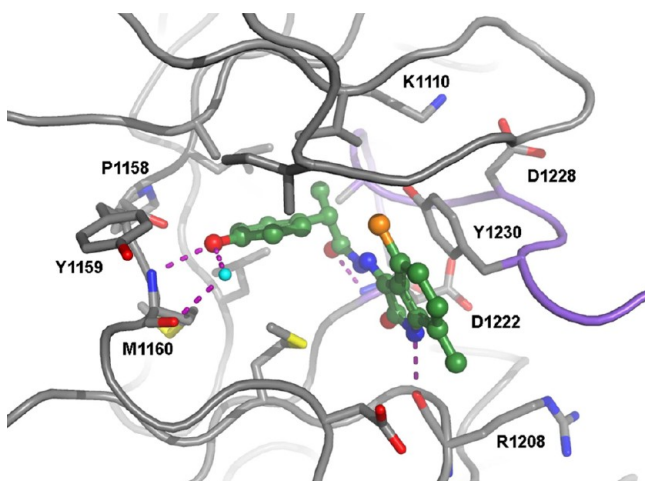

Figure 2. Cocrystal structure of **10** with the nonphosphorylated c-MET.

is not interacting with the hinge as for **8** bound with CDK2. Instead, the phenolic moiety of **10** functions as the hinge binder, with the phenol oxygen bound with the N−H of the hinge Met-1160. Also, a water network links the phenol hydroxyl and Met-1160 carbonyl group. As the molecule makes a turn at the methylene linker, the large coplanar structure of the hydrazide−oxindole allows for strong interactions with the protein backbone. The oxygen of the hydrazide carbonyl group hydrogen bonds with the N−H of Asp-1222, and the N−H of oxindole hydrogen bonds with the carbonyl oxygen of Arg-1208. The intramolecular hydrogen bond between hydrazide and oxindole secures the large coplanar structure and induces strong $\pi-\pi$ interaction with Tyr-1230 of the A-loop. The protein crystal structure of nonphosphorylated c-MET with **10** (Figure 2) reveals a similar conformation as the nonphosphorylated c-MET with **9** (PDB ID 2wkm). A unique β-turn at the beginning of the A-loop is formed, and the c-MET protein adopts an autoinhibitory conformation with the A-loop occupying the binding site for the triphosphate of ATP. This unique c-MET autoinhibitory conformation is consistent with the unphosphorlated apo-c-MET[11] and other c-MET−inhibitor cocrystal structures.[16] Although these c-MET cocrystal structures have the same overall protein fold, the relative position of the A-loop is varied. The A-loop and G-loop (glycine-rich loop) of the c-MET protein in the cocrystal structure of **10** are closer to the inhibitor, and the binding pocket is smaller at the adenine binding site (Figure 3) in comparison with **9**. With the structural overlay of **10** with **9** illustrating the changes (Figure 3), **10** has much reduced molecular weight at the common hinge binding area (phenol group in **10** vs 3-[1-(1*H*-pyrrol-2-yl)meth-(*Z*)-ylidene]-1,3-dihydroindol-2-one) in **9**; however, it has increased molecular weight at the noncommon area, enabling a stronger interaction with the A-loop and the catalytic loop. Because of the strong interaction with the A-loop and reduced interactions at the
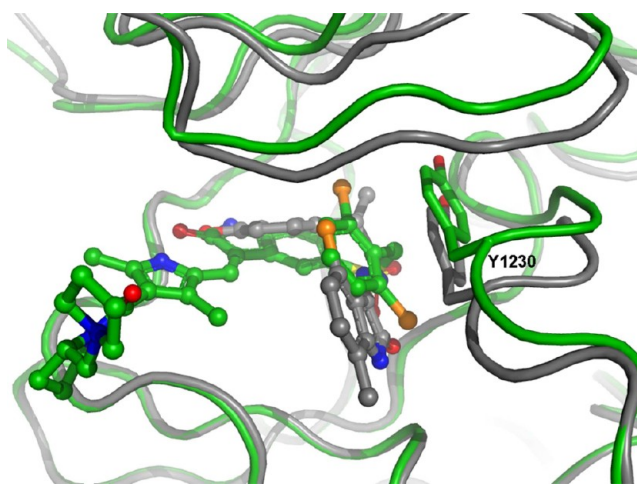

Figure 3. Overlay of c-MET protein structures from cocrystal structures with **10** (gray) and **9** (green).

common kinase inhibitor binding areas, the chemical series of **6** represents a unique scaffold for the c-MET target with high ligand efficiency and selectivity.

Replacement of the Chemically Unstable Oxindole Hydrazide Scaffold. Although the oxindole hydrazide series of **6** is a highly efficient and selective scaffold for c-MET, it was necessary to replace the chemically labile hydrazide linkage with a stable structure. Based on the novel c-MET cocrystal structures with oxindole hydrazide compounds, Vojkovsky et al. fused the hydrazide with oxindole together to form a tetracyclic aromatic scaffold as represented with **11** (Chart 4).[29] The electron deficient tetracyclic fused ring retained the strong $\pi-\pi$ stacking interaction with electron rich Tyr-1230 and could form hydrogen bonds with N−H of Asp-1226 and C=O of Arg-1208. As expected, **11** demonstrated equal potency against c-MET. Although the tetracyclic scaffold solved the chemical stability issue associated with the oxindole hydrazide series, the druggability of the tetracyclic scaffold posed a concern. Zhang et al. chopped the tetracyclic scaffold to the bicyclic triazolotriazine scaffold as represented with **12** (Chart 4).[30] Surprisingly, **12** revealed a better ligand efficiency against c-MET than the tetracyclic scaffold even though with the loss of the hydrogen bond with C=O of Arg-1208. The bicyclic triazolopyrazine scaffold prepared by Cui et al. was slightly less potent than the triazolotriazine scaffold, as demonstrated with compound **13** (Chart 4).[31]

Using insight from the cocrystal structure of an oxindole hydrazide compound with c-MET, the chemically unstable oxindole hydrazide scaffold was successfully replaced with chemically stable triazolotriazine and triazolopyrazine scaffolds that maintained ligand efficacy (Chart 4). Kinase selectivity screening of **12** against a total of 98 protein kinases revealed an exquisite selectivity for c-MET (Supporting Information available). The unique binding mode results in unprecedented selectivity; albeit, **12** is bound at the ATP binding site. The cocrystal structure of **12** bound with nonphosphorylated c-MET confirmed the same binding mode as **10**, however, with a significant movement of A-loop toward the inhibitor for a better $\pi-\pi$ stacking interaction between electron rich Tyr-1230 and the electron deficient triazolotriazine ring (Figure 4). In comparison of the cocrystal structure of **12** with **10**, there is a significant change in the relative position of phenols. In the cocrystal structure of **10** with c-MET, the carbonyl group from

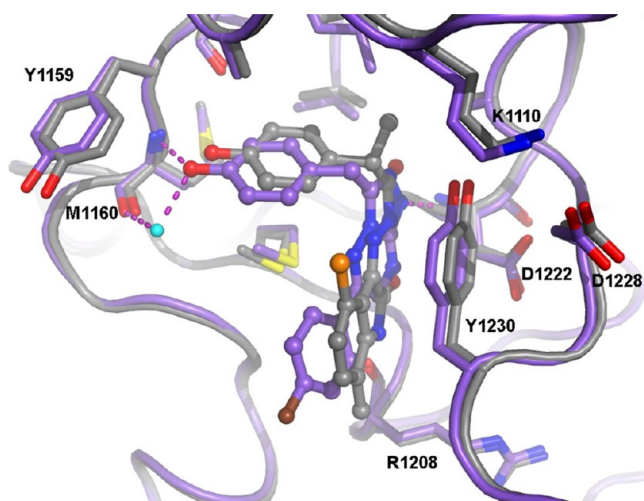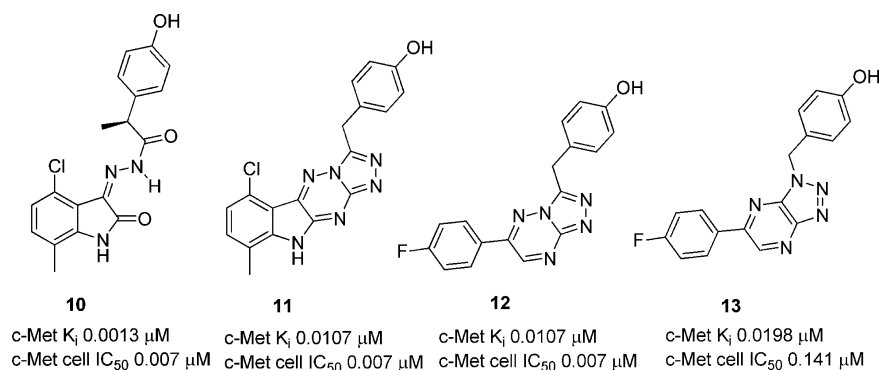**Chart 4. Efforts in the Replacement of the Chemically Unstable Oxindole Hydrazide Scaffold**

10	**11**	**12**	**13**
c-Met K_i 0.0013 μM	c-Met K_i 0.0107 μM	c-Met K_i 0.0107 μM	c-Met K_i 0.0198 μM
c-Met cell IC_{50} 0.007 μM	c-Met cell IC_{50} 0.007 μM	c-Met cell IC_{50} 0.007 μM	c-Met cell IC_{50} 0.141 μM

Figure 4. Overlay of cocrystal structures of **10** (gray) and **12** (purple) bound with the nonphosphorylated c-MET.

hydrazide forms a good hydrogen bond with N−H of Asp-1226, and the carbonyl group of oxindole does not have a direct interaction with the protein backbone; however, the oxindole carbonyl forms an intramolecular hydrogen bond with hydrazide to generate a coplanar structure for a π−π stacking interaction with Tyr-1230. For compound **12**, it is the N-1 of triazolotriazine that forms a hydrogen bond with Asp-1226 from a different angle compared to that of the carbonyl group of the hydrazide in **10**, which places the triazolotriazine ring in a better position for the π−π stacking interaction with Tyr-1230, and the phenol group closer to the hinge for a better hydrophobic interaction with Met-1226 and hydrogen bond interaction with the hinge Met-1160 in a slightly different position in comparison with the phenol in **10**. Without the restriction from the interaction with the C=O of Arg-1208, the 5-phenyl group in **12** orients in a different angle as compared with the oxindole in **10**. Thus, the improved ligand efficiency of the triazolotriazine series is likely due to better π−π stacking interaction from electron rich Tyr-1230 with the electron deficient triazolotriazine ring.
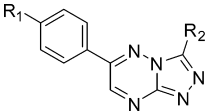
Replacement of the Hinge Binder Phenol. Phenols are well-known to undergo phase II glucuronidation metabolism. Therefore, the next design was focused on the replacement of the phenol hinge binder to optimize the chemical scaffold into a more druggable chemical series. A variety of aromatic groups with heteroatoms as potential hydrogen bond donors and acceptors for the interaction with hinge amino acid residues
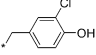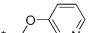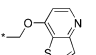
were explored (Table 1). Although the interaction with the A-loop residue Tyr-1230 is important for overall potency and selectivity, it is necessary to use the hinge binder to anchor the molecule into the binding pocket. When the phenol group was removed, **14** was not active against c-MET with a $K_i > 10$ μM. The phenol hydroxyl group in concert with a water mo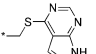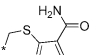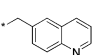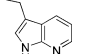lecule formed a hydrogen bond network with hinge residue Met-1160. The replacement of the hydroxyl group with the methoxy group in **15** interrupted the hydrogen bound network, and the activity dropped more than 10-fold in the c-MET cellular assay. **16** with a fluoro group dropped more than 300-fold of activity in the c-MET enzymatic assay. **17** with an ortho-chloro group reduced the potency significantly. **18** with the *N*-substituted pyridin-4(1*H*)-one hinge binder showed a significant reduced potency (6.51 μM), likely because of desolvation penalty from the polar carbonyl group. More exploratory approaches including **19**−**22** with an extended two-atom linker were carried out. **22** demonstrated potent inhibition against c-MET in both enzymatic and cellular assays. **23** and **24**, with the conventional protein kinase hinge binders quinoline and azaindole, were potent c-MET inhibitors. In summary, the phenol hinge binder could be replaced by other kinase hinge binders that retained potency against c-MET. Not surprisingly, the cocrystal structure of **24** with c-MET showed good overlay with the cocrystal structure of **12** with c-MET (Figure 5).

In parallel with the efforts to replace the phenol hinge binder, the ADME properties were optimized. In general, the triazolotriazine chemical series had good caco-2 permeability (data not shown). The metabolic stability in the human microsome varied according to the overall lipophilicity and chemical structures (Figure 6a). However, the series demonstrated high clearance in human hepatocyte even at very low lipophilicity (Figure 6b). The stable compounds in the human hepatocyte assay have *O*- or *N*-substituents at the 7-position of the triazolotriazine core, which indicated that the highly electron deficient triazolotriazine core is subject to non-p450 enzymatic oxidation. From the analyses of cLogD and human metabolic stability (Figure 6), it was concluded that there would be no druggable chemistry space for the triazolotriazine chemical series, and the series was deprioritized.

Optimization to the Clinical Candidate 2-(4-(1-(Quinolin-6-ylmethyl)-1*H*-[1,2,3]triazolo[4,5-*b*]pyrazin-6-yl)-1*H*-pyrazol-1-yl)ethanol (2). Alternatively, the less potent triazolopyrazine series of **13** was explored for potential acceptable ADME properties. The SAR for the phenol replacement of **13** was similar with the triazolotriazine series of **12**, as exemplified with **25**−**27** (Table 2). The 6-substituted quinoline hinge binder in **27** provided good potency against c-

Table 1. Structure Activity Relationship of Phenol Replacements

Compd	R$_1$	R$_2$	cLogD^a	c-MET Ki (μM)^b	c-MET Cell IC$_{50}$ (μM)^b	LipE (IC$_{50}$)^c	HLM CL$_{int, app}$^{d}	HHept CL$_{int, app}$^{e}
12	F	(phenol-OH)	1.43	0.011	0.007	6.72	25.6	93.2
14	F	CH$_3$	0.39	>10	ND	ND	24.9	49.1
15	F	(phenyl-O)	2.08	0.069	0.113	4.86	31.2	59.3
16	F	(phenyl-F)	2.22	0.379	ND	ND	39.2	63.0
17	F	(Cl, phenyl-OH)	1.93	0.0518	0.189	4.79	35.7	62.8
18	F	(N, =O)	0.08	6.51	10.0	5.92	ND	ND
19	F	(O-pyridine)	0.95	7.39	ND	ND	ND	ND
20	F	(thienopyridine-O)	3.14	0.425	>2.5	<3.46	17.4	44.8
21	F	(pyrazolopyrimidine-S)	0.470	0.188	0.52	5.81	28.0	121
22	F	(isothiazole amide)	-0.580	0.002	0.003	9.10	63.3	36.8
23	F	(quinoline)	2.03	0.006	0.005	6.27	63.1	148
24	CN	(azaindole)	1.15	0.004	0.016	6.65	<7.60	64.2

^{a}Calculated logarithm of the octanol/water distribution coefficient at pH 7.4 using ACD pchbat version 9.3. ^{b}Inhibition constants (K_i) and cell IC$_{50}$ were determined as described under Experimental Section. The coefficients of variance were typically less than 20% ($n = 2$). A549 human lung carcinoma cell line was used for the evaluation of the inhibition of autophosphorylation of c-MET. ^{c}LipE (IC$_{50}$) = pIC$_{50}$ − cLogD. ^{d}Human liver microsomal intrinsic clearance (μL/min/mg). ^{e}Human hepatocyte intrinsic clearance (μL/min/million). ND, not determined.

MET and is about 10-fold less potent in the c-MET cellular autophosphorylation assay than the triazolotriazine analogue **23**. However, the metabolic stabilities in both human liver microsomes and the hepatocyte cell were improved even though the lipophilicity of **27** was about 0.71 unit higher than that of **23**, which implies that the triazolopyrazine scaffold was metabolically more stable than triazolotriazine. To further evaluate the potential of the triazolopyrazine series, the analogues **28−32** with a 6-pyrazol-4-yl substitute were synthesized and demonstrated improved LipE and metabolic stabilities. **28** is 57-fold more potent than **25** (0.051 μM over 2.92 μM) in the c-MET cellular assay even though the biochemical potencies (K_i) are similar. The enzymatic assay used the active, autophosphorylated c-MET protein with biochemical potency (K_i) based on the ability of the inhibitor to prevent the phosphorylation of a substrate. The cocrystal structure of **12** with nonphosphorylated c-MET revealed an autoinhibitory conformation of the c-MET protein with the

activation loop occupying the ATP triphosphate binding site. **12** stabilized the nonphosphorylated c-MET in an inactive conformation and resulted in the potent inhibition of c-MET autophosphorylation in the cell. The N-methylpyrazol-4-yl group in **28−32** allows a better coplanar structure with the triazolopyrazine core than the phenyl group in **25−27**. The large coplanar structure facilitates the π−π stacking interaction with Tyr-1230 in the A-loop and led to improved cellular potency. The N-methylpyrazolyl group lowers the LogD by more than two units and results in a significant improvement of LipE, as exemplified with **31**, which has a LipE of 8.32 in comparison of 4.61 for the close analogue **27**. With dramatically lowered lipophilicity, **31** is metabolically stable in both human microsome and hepatocyte. **32** with a quinazoline hinge binder was 7-fold less potent than **31**, as expected with the reduced hydrophobic interaction, reduced hydrogen bond strength, and increased desolvation penalty. In summary, a new druggable chemical series of 6-((1H-[1,2,3]triazolo[4,5-b]pyrazin-1-yl)-
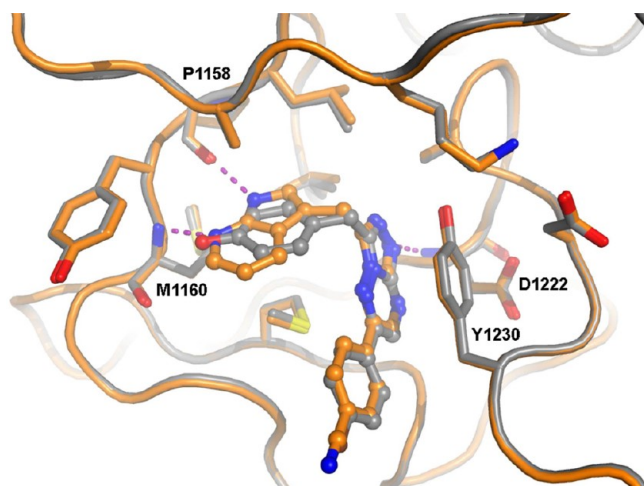
Figure 5. Overlay of cocrystal structures of **24** and **12** with nonphosphorylated c-MET.
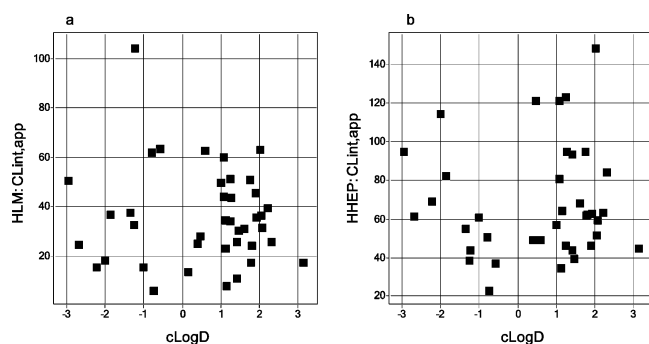

Figure 6. (a) Human liver microsomal clearance (HLM: CLint., app) vs cLogD; (b) Human hepatocyte clearance (HHEP: CLint., app) vs cLogD.

methyl)quinoline was successfully identified to replace the 6-((1*H*-[1,2,3]triazolo[4,5-*b*]pyrazin-1-yl)methyl)quinoline series with good chemical and metabolic stabilities, and c-MET cellular potency.

31 demonstrated good cellular potency against c-MET (IC$_{50}$ = 1 nM), high cellular lipE (8.32), and good human microsome stability and permeability. However, the low solubility of **31** would impact the oral absorption potentially. The cocrystal structure of **12** with c-MET suggested an open space at the 6-pyrazol-yl binding position between the G-loop and the A-loop with a potential interaction with Asp-1164. A variety of polar groups were introduced on the pyrazole to improve the aqueous solubility (Table 3). The unsubstituted pyrazole **33** showed similar potency as **31**, however with even lower solubility and worse metabolic stability. **2** with an ethanolic group showed a comparable potency and ADME properties as **31**. **35** with a carboxyl ethyl group had a similar K_i; however, it was less active in the cell because of low permeability. The introduction of the more lipophilic group 1,1-dimethyl-1-hydroxyethyl in **36** reduced the potency and decreased the metabolic stability. The basic compounds **37** and **38** showed much improved solubility with good potency, metabolic stability, and permeability. **39**, with a 1-ethylpyrrolidin-2-one group, showed reduced potency. **40** and **41**, with secondary basic groups, showed good potency and reduced permeability.

To further define the SAR of the 6-((1*H*-[1,2,3]triazolo[4,5-*b*]pyrazin-1-yl)methyl)quinoline series, a variety of different
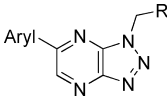
substituents, in addition to the aryl and heteroaryl groups at the 6-position of the triazolopyrazine core, were investigated (Table 4). The essential core **42** with R = H showed a c-MET cellular potency of 253 nM with a LipE of 6.27. **42** has the desired ADME properties (good solubility, metabolic stability, and permeability) for further optimization. **43** with a lipophilic methyl group improved c-MET cellular potency by 3-fold with a similar LipE value (of 6.30) to that for **42**. The amino function in **44** enhanced c-MET cell potency (34 nM), with a much improved LipE of 8.42, and lowered the aqueous solubility to 70.6 μM. **45**, with a lipophilic ethylamino group, further improved c-MET cell potency (6 nM), however with a lower LipE of 8.06, and had a low solubility of 6.57 μM. **46**, with the hydroxyethylamino group, showed a reduced permeability. **47**, with the dimethylaminoethyl amino group, had reduced c-MET cell potency even though the solubility is good. **51**, with the dimethylaminoethyloxy group, showed similar properties as **47**, except better permeability. The cyclic amino substituents at the 6-position showed good potency and ADME properties, as demonstrated with **48−50**. In summary, a variety of substituents at the 6-position of the triazolopyrazine core are tolerated, which provides a good opportunity to optimize potency and pharmaceutical properties.
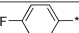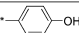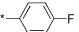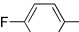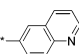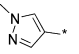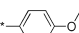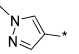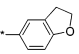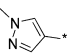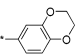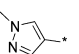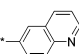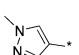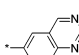
After comprehensive multiparameter lead optimization, a number of compounds were selected for *in vivo* rat PK studies based on potent inhibition of c-MET at both enzymatic and cellular assays and good *in vitro* ADME properties (Table 5). The basic compounds **41** and **48** showed unexpected high *in vivo* rat plasma clearance. Additional compounds with a basic substituent at the 6-position were studied in *in vivo* rat PK and showed similar results to those for **41** and **48** (data not shown). It was suspected that non-p450 related metabolic mechanisms may be linked with the disconnection between the *in vitro* clearance prediction from rat microsomal stability and *in vivo* PK results. **31**, **2**, and **44** showed low to moderate *in vivo* rat clearance, low volume distribution, and good oral bioavailability. **2** showed a better half-life and volume distribution profile and was chosen for further evaluations.

The cocrystal structure of **2** with a nonphosphorylated c-MET kinase domain showed a similar binding mode (Figure 7) to that of the complexes of **12** and **23** with c-MET. The A-loop adopts an autoinhibitory conformation and possesses a strong interaction with **2** via a c-MET characteristic π−π interaction of Tyr-1230 with a triazolopyrazine ring. The quinoline group in **2** is docked into the hinge through a hydrogen bond with Met-1160 and hydrophobic interactions with Ile-1084, Val-1092, Ala-1108, and Met-1211. N-3 on the triazolopyrazine ring forms a hydrogen bond with the N−H of the DFG Asp-1222 residue. Triazolopyrazine is anchored with Tyr-1230 and Met-1211, and the pyrazole moiety forms a hydrogen bond network with a water molecule which interacts with C=O of Tyr-1230 and N−H of Arg-1086. The hydroxyl group from the ethanolic group on the pyrazole forms hydrogen bonds with Asp-1231 and a water molecule.

As expected, **2** demonstrates an exquisite c-MET kinase selectivity (>1000 selectivity to 208 protein kinases).[23] Despite having a similar overall protein conformation in the cocrystal structures of **2** and crizotinib (PDB ID 2wgj) with non-phosphorylated c-MET (Figure 8), crizotinib is less selective, being a c-MET/ALK/ROS/RON inhibitor at the cellular level.[16] Stronger interactions with A-loop Tyr-1230 and also a hydrogen bond to the amide of Asp-1222 may be the basis for the exquisite kinase selectivity of **2**. This hypothesis is

Table 2. Structure Activity Relationship of the Triazolopyrazine Series

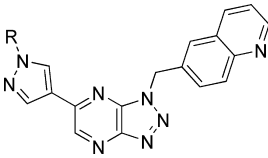| Compd	Aryl	R	cLogD^a	c-MET Ki (µM)^b	c-MET Cell IC$_{50}$ (µM)^b	LipE (IC$_{50}$)^c	HLM CL$_{int, app}$^{d}	HHep CL$_{int, app}$^{e}
13	F—⬡—*	*—⬡—OH	1.86	0.0198	0.141	4.99	42.6	50.0
25	F—⬡—*	*—⬡—O/	2.51	0.073	2.92	3.02	13.4	141
26	F—⬡—*	*—⬡—F	2.65	0.653	10	2.35	ND	ND
27	F—⬡—*	*—⬡⬡N	2.71	0.0048	0.048	4.61	15.4	52.6
28	N/N—⬡—*	*—⬡—O/	0.73	0.082	0.051	6.56	33.5	38.5
29	N/N—⬡—*	*—⬡⬡O	0.74	0.0586	0.0356	6.71	59.9	ND
30	N/N—⬡—*	*—⬡⬡O—O	0.48	0.035	0.146	6.36	47.2	ND
31	N/N—⬡—*	*—⬡⬡N	0.68	0.006	0.001	8.32	5.95	11.8
32	N/N—⬡—*	*—⬡⬡N=N	-0.52	0.044	ND	ND	ND	ND

^{a}Calculated logarithm of the octanol/water distribution coefficient at pH 7.4 using ACD pchbat version 9.3. ^{b}Inhibition constants (K_i) and cell IC$_{50}$ were determined as described in the Experimental Section. The coefficients of variance were typically less than 20% ($n = 2$). The A549 human lung carcinoma cell line was used for the evaluation of the inhibition of autophosphorylation of c-MET. ^{c}LipE (IC$_{50}$) = pIC$_{50}$ − cLogD. ^{d}Human liver microsomal intrinsic clearance (μL/(min mg)). ^{e}Human hepatocyte intrinsic clearance (μL/(min million)). ND, not determined.
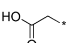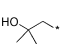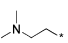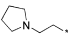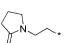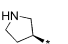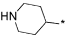
supported by the dramatic decrease in potency of **2** against c-MET when Tyr-1230 is mutated. For example, **2** is almost 1000-fold less active against the c-MET activation loop mutants Y1230C (K_i, 9,400 nM) and Y1235H (K_i, 3,900 nM).[23] However, crizotinib is only 10-fold less potent against Y1230C c-MET.[23]

The different selectivity profiles of **2** and crizotinib indicate the relatively important roles of the Tyr-1230 interaction with the inhibitors. To further explore the nature and the contributions of the Tyr-1230 interaction with **10−13** and crizotinib, the corresponding interaction fragments **A−E** were optimized at the B3LYP/6-31G** level of theory with PBF solvation, and the electronic property calculations were completed on the fragments (Figure 9). The electron density of only the relevant portion of each fragment was revealed for clarity. All the corresponding bond lengths (distances) and bond angles of optimized geometries were in good agreement. The strength of the $\pi-\pi$ stacking interaction of the electron rich Tyr-1230 residue should depend on the electron deficiency of the interacting aromatic system in the kinase inhibitors. Three-dimensional-average local ionization energy (ALIE) superimposed onto a surface of constant electron density (0.01 e/au^3) showing the most positive potential region (deepest blue color for the most electron deficient area) and the most negative potential region (deepest red color for the most electron rich area). The large conjugated coplanar fragment **A** in the initial HTS hit chemical series interacted

with Tyr-1230 efficiently and served as a basis for comparison. In addition to the $\pi-\pi$ stacking interaction with Tyr-1230, fragment **A** formed two pairs of strong hydrogen bonds with the protein backbone, oxindole N—H with the C=O of Arg-1208 and C=O of hydrazide with the N—H of Asp-1222, as shown in the complex of **10** with c-MET (Figure 2). While fragment **B** retained similar interactions as fragment **A** with c-MET protein, fragment **C** showed more blue color (Figure 9), indicating more electron deficiency in the aromatic system for a stronger $\pi-\pi$ stacking interaction with Tyr-1230. Indeed, **12** was equally potent as **11**, however, with a reduced molecular weight, which led to improved ligand efficiency. The stronger interaction with Tyr-1230 of **12** compensated the weaker C—H hydrogen bond with C=O of Arg-1208. **D** had a higher electron density for a weaker $\pi-\pi$ stacking interaction as compared with **C**, which was responsible for a decreased activity of **13** relative to **12** against c-MET. The substituted phenyl fragment **E** in crizotinib showed a significantly different electron potential as compared with fragments **A−D**. The relatively high electron density in **E** led to a weaker interaction with Tyr-1230, and crizotinib lost only 10-fold potency against Y1230C mutant c-MET as compared with **2** (>1000 fold). Crizotinib had additional hydrophobic interactions which were common for other kinases and led to lower selectivity in enzymatic assays. Distinguishing from crizotinib, **2** mainly benefited from the $\pi-\pi$ stacking interaction with Tyr-1230.

Table 3. Structure Activity Relationship of Substituted 6-Pyrazol-4-yl Group

Compd	R	cLogD[a]	c-MET K_i (µM)[b]	c-MET Cell IC_{50} (µM)[b]	LipE (IC_{50})[c]	Solubility (µM)[d]	HLM $CL_{int,app}$[e]	Caco-2 P_{app} AB[f]
31	CH$_3$	0.68	0.006	0.001	8.32	37.8	5.95	11.8
33	H	1.07	0.001	0.006	7.15	5.58	33.9	ND
2	HO⌒⌒*	0.05	0.005	0.004	8.35	22.2	1.48	8.61
35	HO–C(O)–*	-3.21	0.006	0.025	10.81	ND	<7.6	0.003
36	HO–C(CH$_3$)$_2$–*	0.75	0.019	0.017	7.02	26.8	38.0	34.5
37	(CH$_3$)$_2$N⌒*	-0.52	0.020	0.027	8.09	273	19.5	46.5
38	pyrrolidinyl-ethyl*	-0.68	0.0432	0.016	8.48	252	ND	21.9
39	pyrrolidinone-ethyl*	0.37	0.0617	0.091	6.67	93.5	34.4	21.9
40	HN-pyrrolidinyl*	-1.78	0.00614	0.016	9.56	60.4	5.22	3.10
41	HN-piperidinyl*	-1.45	0.0137	0.033	8.93	10.8	<6.0	1.12

[a]Calculated logarithm of the octanol/water distribution coefficient at pH 7.4 using ACD pchbat version 9.3. [b]Inhibition constants (K_i) and cell IC_{50} were determined as described in the Experimental Section. The coefficients of variance were typically less than 20% ($n = 2$). A549 human lung carcinoma cell line was used for the evaluation of the inhibition of autophosphorylation of c-MET. [c]LipE (IC_{50}) = pIC_{50} − cLogD. [d]Kinetic apparent solubility at pH 6.5. [e]Human liver microsomal intrinsic clearance (µL/(min mg)). [e]Caco-2 permeability (10^{-6} cm/s). ND, not determined.

The unique autoinhibitory conformation of c-MET determined the exquisite selectivity profile of **2**.
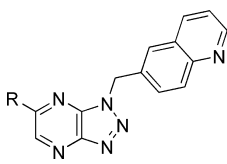
The antitumor efficacy (TGI) and relationship with the inhibition of c-MET autophosphorylation of **2** were evaluated in the c-MET amplified GTL-16 xenograft tumor model (Figure 10). Near complete inhibition of c-MET activity for 24 h is consistent with maximal inhibition of tumor growth (30 and 10 mg/kg, 100−90% TGI), and potent inhibition of c-MET activity for only a portion of the schedule is consistent with significant but submaximal efficacy (3 and 1 mg/kg, 74−64% TGI). These results suggest that near-complete inhibition of c-MET autophosphorylation (>90% inhibition) for the duration of the administration schedule is necessary to maximize therapeutic benefit. The antitumor efficacies in other tumor models and the mechanisms of antitumor efficacy are published elsewhere.[32]
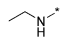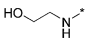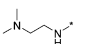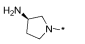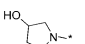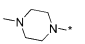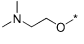
2 was a weak base with a pK_a value of 4.6, resulting in a pH dependent aqueous solubility. The solubility of the crystal mesylate salt of **2** at 25 °C in simulated gastric fluid (SGF, pH 1.2) was >2.0 mg/mL. In sodium phosphate buffer (pH 6.5, 0.05 M), the solubility was significantly lower, at 0.6 µg/mL. **2** showed high metabolic stability in human liver microsomes, moderate human plasma protein binding (84%), and high permeability in the Caco-2 cell assay. Biotransformation mediated by CYP3A4 was likely to be the major clearance mechanism for **2**. **2** was not an inhibitor of CYP1A2, 2C8,

2C19, 2D6, and 3A4 (IC_{50} >30 µM) in human liver microsomes; however, it moderately inhibited CYP2C9 (IC_{50} ~ 5 µM). **2** was well absorbed in animals with a projected fraction absorbed of >90% in humans. The CL_{blood} and V_{ss} values in humans were predicted to be 4−8 mL/(min kg) and 2.2 L/kg, respectively.[33] The human PK profile was evaluated in phase I clinical studies. After a single oral administration at the dose of 30 mg to healthy volunteers, **2** was rapidly and extensively absorbed with a mean C_{max} of 0.24 µg/mL at 1.2 h postdose. Thereafter, **2** declined multiexponentially, with an apparent mean $t_{1/2}$ of 6.6 h. The mean area under the plasma concentration−time curve was 0.81 (µg h)/mL, which corresponded to an oral clearance of 9 mL/(min kg).[33]

2 was negative in the Biolume Ames assay in the presence or absence of rat liver S9 metabolic activation. In the CHO cell micronucleus assay, **2** was also negative in the absence and presence of S9. **2** had a low risk of QT prolongation based on the hERG patch clamp studies (IC_{50} > 30 µM). **2** also displayed an acceptable safety profile in exploratory toxicity studies.

Taken on the whole, **2** was a potent and highly selective c-MET inhibitor *in vitro* and *in vivo*. On the basis of the pharmacologic and pharmacokinetic properties, a good safety margin in preclinical animal studies, and a low risk for clinically relevant drug−drug interaction, **2** was selected for human clinic studies for cancer patients with abnormal c-MET activation.

Table 4. Structure Activity Relationship of 6-Substituents on ((1H-[1,2,3]Triazolo[4,5-b]pyrazin-1-yl)methyl)quinoline

Compd	R	cLogD[a]	c-MET K_i (μM)[b]	c-MET Cell IC$_{50}$ (μM)[b]	LipE (IC$_{50}$)[c]	Solubility (μM)[d]	HLM CL$_{int,app}$[e]	Caco-2 P$_{app}$ AB
42	H	0.33	0.068	0.253	6.27	511	<8.0	40.5
43	CH₃	0.79	0.034	0.082	6.30	363	18.5	35.4
44	NH₂	-0.95	0.015	0.034	8.42	70.6	<7.6	26.5
45		0.24	0.004	0.005	8.06	6.57	20.4	20.5
46		-0.93	0.009	0.027	8.50	32.2	NA	2.79
47		-2.12	0.14	0.165	8.90	543	<7.6	2.08
48		-1.73	0.007	0.014	9.58	288	<7.6	16.8
49		-1.21	0.0209	0.053	8.49	483	<7.6	24.1
50		-0.01	0.0373	0.025	7.61	398	24.1	25.1
51		1.15	0.106	0.166	5.63	488	4.65	25.9

[a]Calculated logarithm of the octanol/water distribution coefficient at pH 7.4 using ACD pchbat version 9.3. [b]Inhibition constants (K_i) and cell IC$_{50}$ were determined as described in the Experimental Section. The coefficients of variance were typically less than 20% ($n = 2$). The A549 human lung carcinoma cell line was used for the evaluation of the inhibition of autophosphorylation of c-MET. [c]LipE (IC$_{50}$) = pIC$_{50}$ − cLogD. [d]Kinetic apparent solubility at pH 6.5. [e]Human liver microsomal intrinsic clearance (μL/(min mg)). [f]Caco-2 permeability (10^{-6} cm/s). ND, not determined.

Table 5. In Vivo Rat Pharmacokinetic Properties

compd	MW	pK_a[a]	cLogD[b]	eLogD[c]	CL$_{plasma}$ (mL/(min kg))	V_{ss} (L/kg)	$T_{1/2}$ (h)	F_{oral} (%)
31	342	4.66	0.68	1.29	9.7	0.42	1.5	76
2	372	4.66	0.05	1.38	8.2	1.6	3.7	71
41	411	10.2	−1.45	ND	81.7	27	5.0	BQL
44	277	4.66	−0.95	1.23	26.7	0.95	1.6	75
48	346	8.52	−1.73	0.86	83.4	3.6	0.9	BQL

[a]Calculated ionization constant of a molecule using ACD pchbat version 9.3. [b]Calculated logarithm of the octanol/water distribution coefficient at pH 7.4 using ACD pchbat version 9.3. [c]Experimentally measured bilayer participating coefficient at pH 7.4. BQL: below quantification level.

■ CHEMISTRY

12 and **14−24** were prepared according to Scheme 1. **52a−b** were prepared according to the literature procedure[34] and were coupled with a carboxylic acid in the presence of the coupling reagents hydroxybenzotriazole (HOBT) and 1-ethyl-3-(3-dimethylaminopropyl) carbodiimide (EDC) in N-methylpyrrolidone (NMP) at ambient temperature. After the completion of the coupling reaction, the reaction mixture was microwaved at 170 °C until the formation of the triazolotriazine core was completed.

13 and **25−33** were prepared according the general three-step procedure in Scheme 2. The substituted amine replaced the 3-bromo group of 3,5-dibromopyrazin-2-amine in n-butanol with the presence of diisopropylethylamine (DIPEA) under

reflux to provide the N^2-substituted 6-bromo-pyrazine-2,3-diamine **54**. The Sandmeyer reaction using isoamyl nitrite in dimethylformamide (DMF) closed the ring to provided the key intermediate **55**. **13** and **25−33** were obtained with conventional Suzuki coupling conditions.

The synthesis of **2** was summarized in Scheme 3. **58** was prepared under conventional alkylation conditions with Cs$_2$CO$_3$ as a base in DMF solvent at 70 °C. The boronic ester was introduced via metalation with i-PrMgCl and then quenched with the boronic ester reagent. **2** was prepared via conventional Suzuki coupling conditions followed by deprotection under hydrogen chloride acidic conditions.

The general alkylation condition was used to introduce various substituted groups on the pyrazole ring of **33**, as illustrated in Scheme 4.
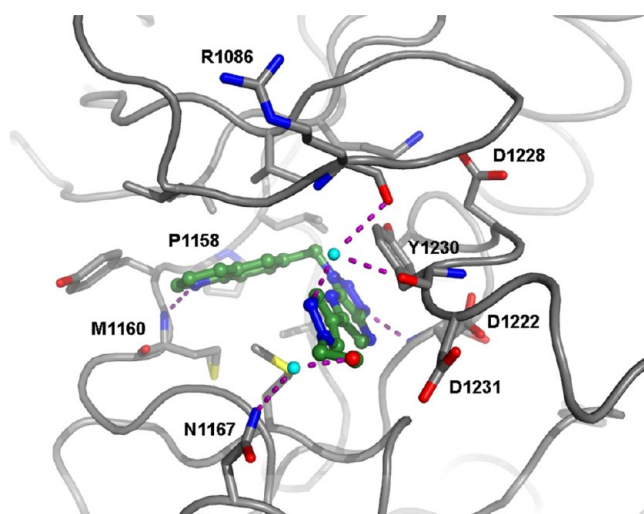
Figure 7. Cocrystal structure of **2** with nonphosphorylated c-MET.
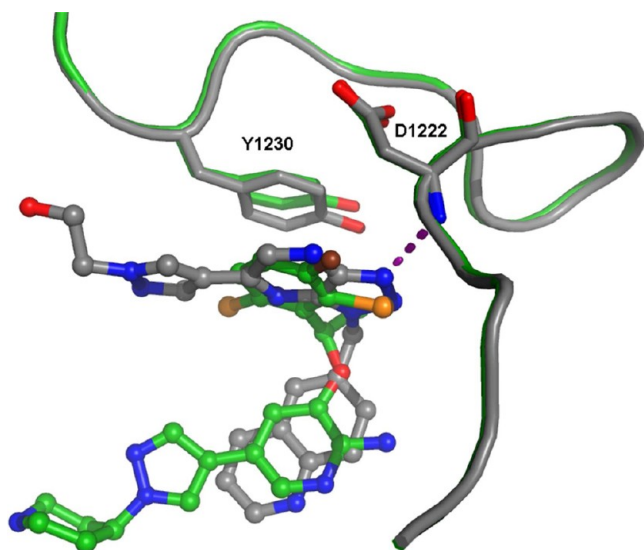
Figure 8. Overlay of cocrystal structures of **2** (gray) and crizotinib (green) with nonphosphorylated c-MET.

The preparation of **42–51** was summarized in Scheme 5. Hydrogenation of **55d** gave **42**. The methyl group was introduced from **55d** under palladium catalyst to provide **43**. **44** was prepared with ammonia under microwave thermal conditions. A variety of substituted amino groups were introduced with potassium carbonate as a base under microwave thermal conditions to provide **45–50**. The alkoxy compound **51** was prepared with triethylamine as a base under microwave thermal conditions.

■ **CONCLUSIONS**

Oxindole hydrazide **6** with an unusual kinase selectivity profile was a hit in a c-MET receptor tyrosine kinase HTS campaign. The selectivity profile could not be rationalized with the conventional oxindole kinase inhibitor binding mode in which the oxindole bound to the hinge region of the ATP binding site. A cocrystal structure of the related oxindole hydrazide compound **10** with the nonphosphorylated c-MET kinase domain confirmed a unique binding mode with a phenol group bound to the hinge region and the oxindole hydrazide portion
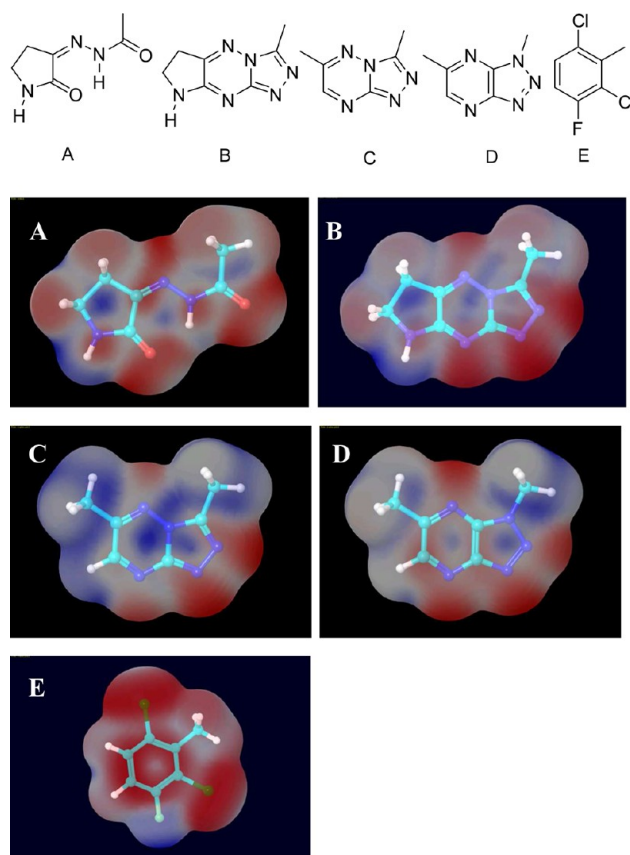
Figure 9. Electronic property calculations of fragments **A–E**.

having a strong interaction with the activation loop. Based on insight from the cocrystal structure, a tetracyclic mimic, represented with **11**, was designed, and it demonstrated increased potency and the same selectivity profile. Further optimization of druglike properties resulted in a triazolotriazine series, as represented with **12**. The quinoline group was designed to replace the phenol group as a hinge binder, and the triazolopyrazine ring was used to replace the metabolically labile triazolotriazine ring to generate a new chemically and metabolically stable scaffold, as illustrated with compound **23**. Medicinal chemistry optimization of the triazolopyrazine series led to the discovery of **2**, which demonstrated potent inhibition of c-MET in both *in vitro* cell assays and *in vivo* target modulation studies. In preclinical studies, **2** had significant tumor growth inhibition, good oral PK properties, and an acceptable safety margin. **2** is an ATP competitive inhibitor and bound at the adenine binding pocket. However, the kinase selectivity screens against 208 different protein kinases indicated an exquisite selectivity profile associated with **2**, which could be explained with the unique binding topography of the c-MET kinase domain. **2** was advanced into phase I clinical studies for oncology indications.

The successes of imatinib for chronic myeloid leukemia patients having BCR-ABL abnormal gene, erlotinib for advanced nonsmall cell lung cancer patients having EGFR mutations, and crizotinib for lung cancer patients having EML4-ALK fusion gene illustrate the importance to identify the disease-driven oncogene for the effective treatment of cancers. However, genetic intratumor heterogeneity presents major challenges to personalized medicine and can lead to tumor adaptation and resistance to treatment.[35] Frequently, there are
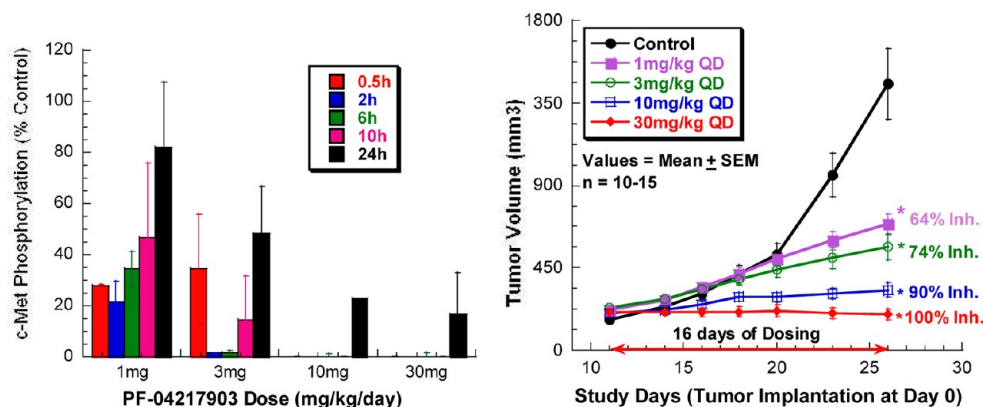
Figure 10. Tumor growth inhibition of **2** in the GTL-16 xenograft tumor model.

Scheme 1[a]

52a: R' = F
52b: R' = CN

53

12, 14-24
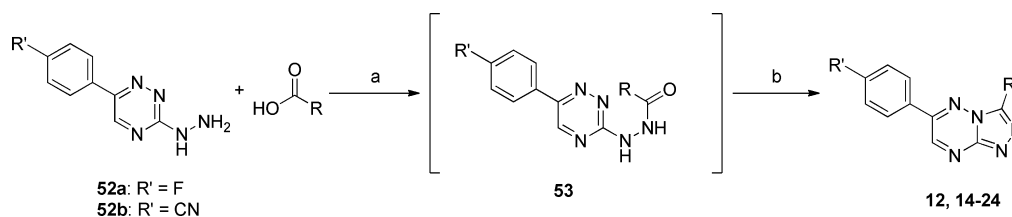
[a]Reagents and conditions: (a) HOBT, EDC, NMP, ambient temperature, 1–2 h; (b) microwave at 170 °C, 0.5 h or longer.

Scheme 2[a]

54a: R = 4-hydroxyphenyl
54b: R = 4-methoxyphenyl
54c: R = 4-fluorophenyl
54d: R = quinolin-6-yl
54e: R = 2,3-dihydrobenzofuran-5-yl
54f: R = 2,3-dihydrobenzo[b][1,4]dioxin-6-yl

55a: R = 4-hydroxyphenyl
55b: R = 4-methoxyphenyl
55c: R = 4-fluorophenyl
55d: R = quinolin-6-yl
55e: R = 2,3-dihydrobenzofuran-5-yl
55f: R = 2,3-dihydrobenzo[b][1,4]dioxin-6-yl

13, 25-33
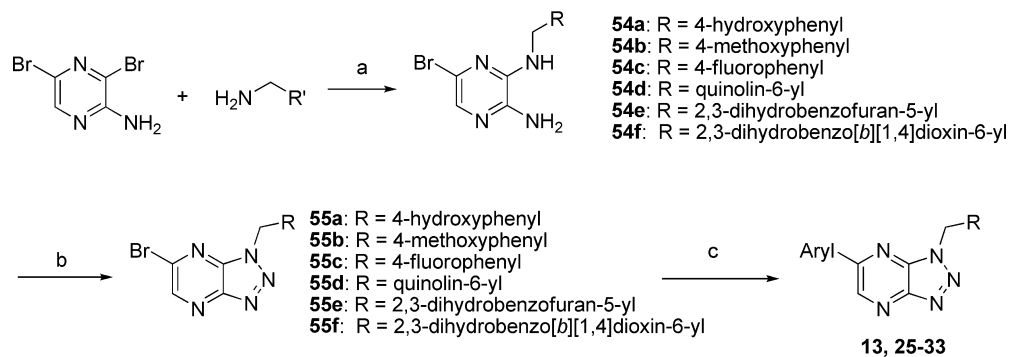
[a]Reagents and conditions: (a) n-butanol, DIPEA, reflux, 48 h; (b) isoamyl nitrite, DMF, ambient temperature, overnight, 70 °C to the completion; (c) Pd(dppf)Cl$_2$·CH$_2$Cl$_2$, Na$_2$CO$_3$, DME/H$_2$O, 80 °C, 3.5 h.

more than one abnormal genes associated with a particular cancer. The design of a kinase inhibitor targeting a specific subset of kinases may not be practical because of the diversified kinase structures and intrinsic kinase activities. The combination of drugs targeting specific mechanisms associated with the disease may represent the future of cancer treatment. Highly selective kinase inhibitors should provide good opportunities to combine together for maximum efficacy and minimum toxicity. **2**, distinguished from multitargeted c-MET inhibitors currently in clinical trials, will provide opportunities to validate the role of the c-MET target in tumor development, and it could be used as a single agent or combined effectively with other agents for the treatment of cancers.

■ EXPERIMENTAL SECTION

General Methods for Chemistry. All reagents and solvents were used as purchased from commercial sources. Reactions were carried out under nitrogen atmosphere unless otherwise indicated. Silica gel chromatography was done using the appropriate size Biotage prepacked silica filled cartridges. NMR spectra were generated on a Bruker 300 or 400 MHz instrument and obtained as CDCl$_3$ or DMSO-d_6 or MeOH-d_4 solutions (reported in ppm), using CDCl$_3$ as the reference standard (7.27 ppm), DMSO-d_6 (2.50 ppm), and MeOH-d_4 (3.31 ppm). Multiplicities were given as s (singlet), br s (broad singlet), d (doublet), t (triplet), dt (double of triplets), and m (multiplet). Mass spectral data (APCI) was gathered on an Agilent 1100 LC with MSD (Agilent model G1946B upgraded to D model) single-quadrupole mass spectrometric detectors running with an atmospheric pressure chemical ionization source. The LC instrument includes a binary pump (Agilent model G1312A) with an upper pressure limit of 400 bar attached to an autosampler (Agilent model G1313A) which uses an external tray for sample submission. The column compartment (Agilent model G1316A) is attached to a diode array (Agilent model G1315A). The instrument acquisition and data handling were done with ChemStation rev B.02.01. The purity measurements were done by measuring peak area at 254 nm, 224 nm, and total ion chromatogram. To evaluate the purity of each peak, the UV−vis spectrum from 190 to 700 nm at a step size of 2 nm and mass spectrum scan from 150 to 850 amu with a cycle time of 0.29 cycle/s

Scheme 3. [a]
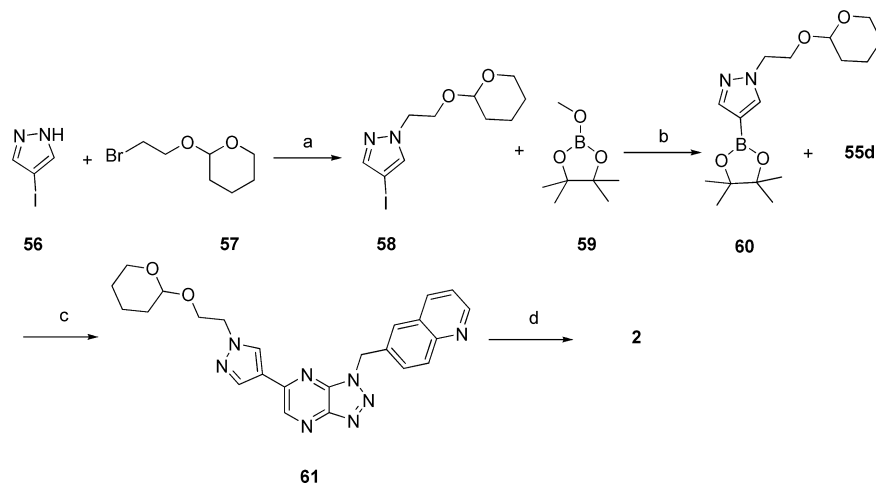
[a] Reagents and conditions: (a) Cs_2CO_3, DMF, 70 °C, 16 h; (b) i-PrMgCl, THF, 0 °C to RT, 1 h; (c) Pd(dppf)Cl_2·CH_2Cl_2, Cs_2CO_3, DME/H_2O, 80 °C, 16 h; (d) 4 N HCl/dioxane, CH_2Cl_2, RT.

Scheme 4. [a]
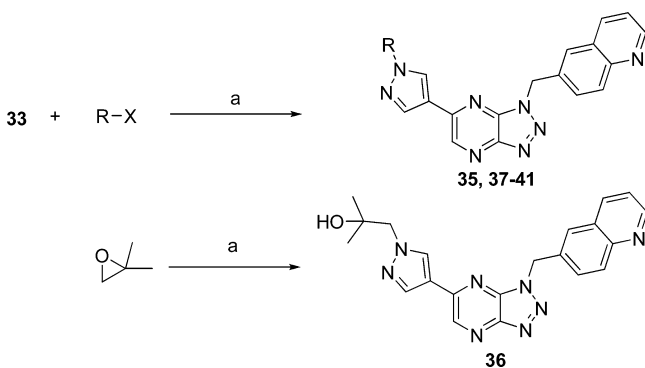
[a] Reagents and conditions: (a) Cs_2CO_3, DMF, 80 °C, overnight.

was performed. Retention times (RT) were in minutes, and purity was calculated as percentage of total area. Two HPLC methods were utilized for purity. Method A: Waters Acquity UPLC BEH C18 column, 1.7 μm, 2.1 mm × 100 mm, column temperature 80 °C; solvent A: water (0.1% formic acid and 0.05% ammonium formate); solvent B: methanol (0.1% formic acid and 0.05% ammonium formate); gradient: 5−95%B in 10 min, 95%B 10−12 min; flow rate 0.6 mL/min. Method B: EclipsXDB C8 column, 3.5 μm, 4.6 mm × 50 mm, column temperature 40 °C; solvent A: water (5% ACN, 2 mM ammonium acetate, 0.1% acetic acid); solvent B: ACN (5% H_2O, 2 mM ammonium acetate, 0.1% acetic acid); gradient: 20−85%B (0.0−2.5 min), 85−95%B (2.5−3.5 min), 95%B (5 min); flow rate = 0.8 mL/min. Compound purity was determined by combustion analysis (Atlantic Microlabs, Inc.) or high pressure liquid chromatography (HPLC) with a confirming purity of ≥95% for all final biological testing compounds.

General Procedure A for the Preparation of Triazolotriazine Compounds. To a solution of substituted acetic acid (1 molar equiv),

Scheme 5. [a]
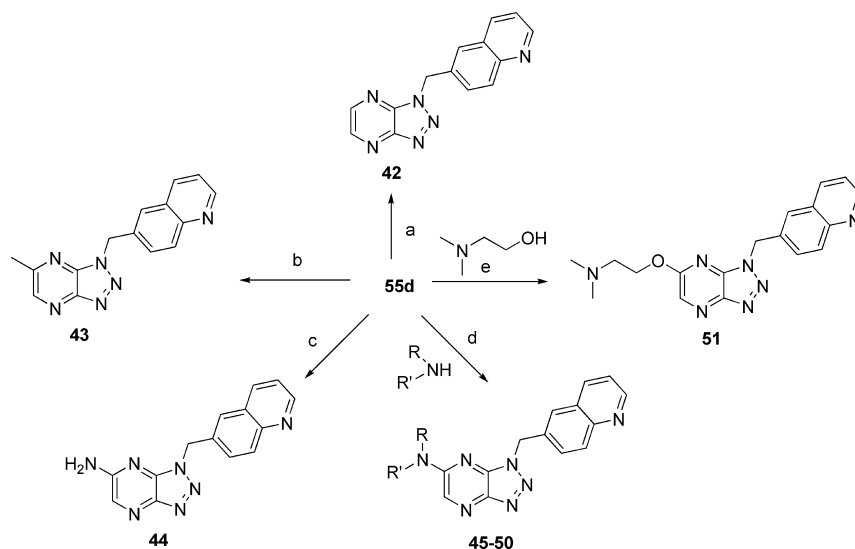
[a] Reagents and conditions: (a) H_2, Pd/C, MeOH/AcOH/EtOAc, 18 h; (b) MeB(OH)$_2$, Pd(PPh$_3$)$_2$Cl$_2$, Na$_2$CO$_3$, DME/H_2O, 80 °C, 16 h; (c) concentrated ammonia−water solution, microwave at 100 °C, 1 h; (d) K_2CO_3, i-PrOH, microwave at 80 °C, 20 min; (e) Et$_3$N, n-BuOH, microwave at 120 °C, 20 min.

HOBT (1 molar equiv), and EDC (1.1 molar equiv) in NMP (0.25 M) in a microwave reaction vessel was added **52a** or **52b** (1.0 molar equiv). The suspension was stirred at ambient temperature until a clear solution was obtained and a complete conversion to the intermediate **53** was observed by LC-MS (it took 1–2 h). The reaction vessel was then microwaved at 170 °C for 30 min or longer until over 90% conversion to the final product was observed in LC-MS. The reaction solution was diluted with ethyl acetate, washed with water 5 times to remove the reaction solvent, and washed with brine. The organic solution was dried over Na$_2$SO$_4$, filtered, and concentrated. The crude product was purified on a silica gel column, eluting with EtOAc–hexane (50% to 100% EtOAc), or purified on a reversed phase preparative HPLC, eluting with 10–40% (30 min) acetonitrile in water (containing 0.1% acetic acid). A highly crystalline solid product was obtained.

3-(4-Fluorobenzyl)-6-(4-fluorophenyl)[1,2,4]triazolo[4,3-b]-[1,2,4]triazine (16). To a solution of (4-fluorophenyl)acetic acid (154.1 mg, 1.0 mmol), HOBT (1 molar equiv), and EDC (1.1 molar equiv) in NMP (4.0 mL) in a microwave reaction vessel was added [6-(4-fluorophenyl)[1,2,4]triazin-3-yl]hydrazine (205.2 mg, 1.0 mmol). The suspension was stirred at ambient temperature for overnight. LC-MS showed a complete conversion to the hydrazide intermediate. The reaction vessel was then microwaved at 170 °C for 30 min and LC-MS showed about 30% product was formed, at 170 °C for an additional 30 min and 60% product, and at 170 °C for another 30 min and >90% product was formed from LC-MS. The reaction solution was diluted with ethyl acetate, washed with water for 5 times to remove the reaction solvent, and washed with brine. The organic solution was dried over Na$_2$SO$_4$, filtered, and concentrated. The crude product was purified on a silica gel column eluting with EtOAc–hexane (50% to 100% EtOAc) to provide a yellow crystalline solid product (110 mg, 34% yield); LC-MS m/z 324 (M + H)$^+$; ^{1}H NMR (400 MHz, DMSO-d_6) δ 9.35 (s, 1H), 8.25 (dd, J = 5.43, 8.97 Hz, 2H), 7.41–7.56 (m, 4H), 7.16 (t, J = 8.97 Hz, 2H), 4.57 (s, 2H); HPLC purity (method A): RT 11.78, >99%.

Compounds **12** and **14**–**24** were prepared according to the general procedure A.

4-((6-(4-Fluorophenyl)[1,2,4]triazolo[4,3-b][1,2,4]triazin-3-yl)methyl)phenol (12). LC-MS m/z 322 (M + H)$^+$; ^{1}H NMR (400 MHz, DMSO-d_6) δ 9.34 (s, 1H), 9.30 (s, 1H), 8.25 (dd, J = 5.31, 8.84 Hz, 2H), 7.50 (t, J = 8.84 Hz, 2H), 7.19 (d, J = 8.34 Hz, 2H), 6.70 (s, 2H), 4.43 (s, 2H); HPLC purity (method A): RT 11.22, >99%.

6-(4-Fluorophenyl)-3-methyl[1,2,4]triazolo[4,3-b][1,2,4]-triazine (14). LC-MS m/z 230 (M + H)$^+$; ^{1}H NMR (400 MHz, DMSO-d_6) δ 9.34 (s, 1H), 8.23–8.30 (m, 2H), 7.46–7.53 (m, 2H), 2.75 (s, 3H); HPLC purity (method A): RT 10.96, >99%.

6-(4-Fluorophenyl)-3-(4-methoxybenzyl)[1,2,4]triazolo[4,3-b][1,2,4]triazine (15). LC-MS m/z 336 (M + H)$^+$; ^{1}H NMR (400 MHz, DMSO-d_6) δ 9.34 (s, 1H), 8.25 (dd, J = 5.43, 8.97 Hz, 2H), 7.50 (t, J = 8.97 Hz, 2H), 7.33 (d, J = 8.84 Hz, 2H), 6.84–6.93 (m, 2H), 4.49 (s, 2H), 3.71 (s, 3H); HPLC purity (method A): RT 11.71, >99%.

2-Chloro-4-((6-(4-fluorophenyl)[1,2,4]triazolo[4,3-b][1,2,4]-triazin-3-yl)methyl)phenol (17). LC-MS m/z 356 (M + H)$^+$; ^{1}H NMR (400 MHz, DMSO-d_6) δ 10.07 (s, 1H), 9.35 (s, 1H), 8.18–8.31 (m, 2H), 7.44–7.53 (m, 2H), 7.41 (d, J = 2.02 Hz, 1H), 7.16 (dd, J = 2.02, 8.34 Hz, 1H), 6.90 (d, J = 8.34 Hz, 1H), 4.46 (s, 2H); HPLC purity (method A): RT 11.45, >95%.

1-((6-(4-Fluorophenyl)[1,2,4]triazolo[4,3-b][1,2,4]triazin-3-yl)methyl)pyridin-4(1H)-one (18). LC-MS m/z 323 (M + H)$^+$; ^{1}H NMR (400 MHz, DMSO-d_6) δ 9.44 (s, 1H), 8.31 (dd, J = 5.43, 8.97 Hz, 2H), 7.78–7.86 (m, 2H), 7.52 (t, J = 8.84 Hz, 2H), 6.08–6.18 (m, 2H), 5.76 (s, 2H); HPLC purity (method A): RT 9.13, >95%.

6-(4-Fluorophenyl)-3-((pyridin-3-yloxy)methyl)[1,2,4]-triazolo[4,3-b][1,2,4]triazine (19). LC-MS m/z 323 (M + H)$^+$; ^{1}H NMR (400 MHz, CDCl$_3$) δ 9.08 (s, 1H), 8.49 (br s, 1H), 8.31 (br s, 1H), 7.99–8.12 (m, 2H), 7.55 (dd, J = 8.46, 1.89 Hz, 1H), 7.29–7.37 (m, 3H), 5.75 (s, 2H); HPLC purity (method B): RT 2.71, >95%.

6-(4-Fluorophenyl)-3-((thieno[3,2-b]pyridin-7-yloxy)-methyl)[1,2,4]triazolo[4,3-b][1,2,4]triazine (20). LC-MS m/z 379 (M + H)$^+$; ^{1}H NMR (400 MHz, DMSO-d_6) δ 9.41 (s, 1H), 8.23–8.35

(m, 2H), 8.18 (d, J = 7.58 Hz, 1H), 8.05 (d, J = 5.56 Hz, 1H), 7.67 (d, J = 5.56 Hz, 1H), 7.49–7.55 (m, 2H), 6.16 (d, J = 7.58 Hz, 1H), 6.13 (s, 2H); HPLC purity (method B): RT 2.08, >95%.

6-(4-Fluorophenyl)-3-((1H-pyrazolo[3,4-d]pyrimidin-4-ylthio)methyl)[1,2,4]triazolo[4,3-b][1,2,4]triazine (21). LC-MS m/z 380 (M + H)$^+$; ^{1}H NMR (400 MHz, DMSO-d_6) δ 14.19 (br s, 1H), 9.39 (s, 1H), 8.81 (s, 1H), 8.36 (s, 1H), 8.11–8.17 (m, 2H), 7.39–7.48 (m, 2H), 5.34 (s, 2H); HPLC purity (method A): RT 11.23, >95%.

3-(((6-(4-Fluorophenyl)[1,2,4]triazolo[4,3-b][1,2,4]triazin-3-yl)methyl)thio)-5-(methylamino)isothiazole-4-carboxamide (22). LC-MS m/z 417 (M + H)$^+$; ^{1}H NMR (400 MHz, DMSO-d_6) δ 9.39 (s, 1H), 8.19–8.27 (m, 2H), 8.02 (br s, 1H), 7.44–7.55 (m, 2H), 7.09 (br s, 2H), 4.99 (s, 2H), 2.83 (s, 3H); HPLC purity (method B): RT 2.71, >95%.

6-((6-(4-Fluorophenyl)[1,2,4]triazolo[4,3-b][1,2,4]triazin-3-yl)methyl)quinoline (23). LC-MS m/z 357 (M + H)$^+$; ^{1}H NMR (400 MHz, DMSO-d_6) δ ppm 9.37 (s, 1H), 8.93 (d, J = 4.04 Hz, 1H), 8.44 (d, J = 8.59 Hz, 1H), 8.22–8.29 (m, 2H), 8.01–8.06 (m, 2H), 7.88 (d, J = 9.09 Hz, 1H), 7.60 (dd, J = 8.21, 4.17 Hz, 1H), 7.46–7.51 (m, 2H), 4.81 (s, 2H); HPLC purity (method B): RT 2.83, >95%

4-(3-((1H-Pyrrolo[2,3-b]pyridin-3-yl)methyl)[1,2,4]triazolo-[4,3-b][1,2,4]triazin-6-yl)benzonitrile (24). LC-MS m/z 353.0 (M + H)$^+$; ^{1}H NMR (400 MHz, DMSO-d_6) δ 11.51 (br s, 1H), 9.39 (s, 1H), 8.37 (d, J = 8.59 Hz, 2H), 8.20 (dd, J = 1.52, 4.55 Hz, 1H), 8.12 (d, J = 8.84 Hz, 2H), 8.04–8.08 (m, 1H), 7.49 (d, J = 2.27 Hz, 1H), 7.06 (dd, J = 4.67, 7.96 Hz, 1H), 4.69 (s, 2H); HPLC purity (method A): RT 10.84, >95%.

General Procedure B for the Preparation of Triazolopyr-azine Compounds 13 and 25–33. Step 1: 6-Bromo-N^2-(quinolin-6-ylmethyl)pyrazine-2,3-diamine (54d). 3,5-Dibromopyrazin-2-amine (21.8 g, 0.086 mol), quinolin-6-ylmethaneamine (13.6 g, 0.086 mol), and diisopropylethylamine (16.5 mL, 0.0946 mol) were dissolved in n-BuOH (150 mL). The reaction mixture was refluxed for 2 days and evaporated. The residue was treated with CH$_2$Cl$_2$ (100 mL) and water (200 mL). The obtained mixture was vigorously stirred for 20 min. The formed precipitate was separated by filtration, washed with water, and dried to afford **54d** (21 g, 74%) as a colorless solid; LC-MS m/z 330 (M + H)$^+$; ^{1}H NMR (400 MHz, DMSO-d_6) δ 8.87 (dd, J = 1.52, 4.04 Hz, 1H), 8.35 (d, J = 7.83 Hz, 1H), 8.01 (d, J = 8.59 Hz, 1H), 7.90 (s, 1H), 7.75 (dd, J = 1.89, 8.72 Hz, 1H), 7.52 (dd, J = 4.17, 8.21 Hz, 1H), 7.22 (s, 1H), 7.17 (t, J = 5.43 Hz, 1H), 6.25 (s, 2H), 4.71 (d, J = 5.56 Hz, 2H).

Step 2. 6-((6-Bromo-1H-[1,2,3]triazolo[4,5-b]pyrazin-1-yl)-methyl)quinoline (55d). **54d** (77 g, 0.233 mol) was dissolved in DMF (2 L). The solution was cooled to 0 °C. A solution of isoamyl nitrite (32.76 g, 0.28 mol) in DMF (500 mL) was added dropwise for 90 min. The reaction mixture was stirred at room temperature overnight and then heated to 70 °C until the reaction was complete. The reaction mixture was cooled to room temperature and concentrated in high vacuum. The residue was crystallized from THF to afford **55d** (55.7 g, 70%) as brown crystals; LC-MS m/z 341 (M + H)$^+$; ^{1}H NMR (400 MHz, DMSO-d_6) δ 9.01 (s, 1H), 8.91 (dd, J = 1.77, 4.29 Hz, 1H), 8.35 (d, J = 7.58 Hz, 1H), 8.03 (d, J = 8.59 Hz, 1H), 7.94 (d, J = 1.26 Hz, 1H), 7.78 (dd, J = 2.02, 8.59 Hz, 1H), 7.54 (dd, J = 4.29, 8.34 Hz, 1H), 6.19 (s, 2H); Anal. Calcd for C$_{14}$H$_9$N$_6$Br: C, 49.29; H, 2.66; N, 24.63. Found: C, 49.37; H, 2.79; N, 24.41.

Step 3: 6-((6-(4-Fluorophenyl)-1H-[1,2,3]triazolo[4,5-b]-pyrazin-1-yl)methyl)quinoline (27). A mixture of DME (3.0 mL) and aqueous Na$_2$CO$_3$ (1.0 M, 0.88 mL) was degassed by bubbling in argon for 10 min. The mixture was transferred via syringe to a vial containing **55d** (100 mg, 0.29 mmol), 4-fluorophenylboronic acid (45 mg, 0.32 mmol), and Pd(dppf)C$_{12}$·CH$_2$C$_{12}$ (6.2 mg, 0.01 mmol). The vial was capped and heated to 80 °C for 3.5 h. The crude reaction mixture was diluted with dichloromethane and then washed with water. The dichloromethane solution was dried over Na$_2$SO$_4$, filtered, and concentrated. The residue was purified via column chromatography, eluting with ethyl acetate and dichloromethane to provide **27** (77 mg, 74%). LC-MS m/z 357 (M + H)$^+$; ^{1}H NMR (400 MHz, DMSO-d_6) δ 9.19–9.24 (m, 1H), 8.98 (dd, J = 4.29, 1.52 Hz, 1H), 8.64 (s, 1H), 8.52 (d, J = 7.83 Hz, 1H), 8.30 (s, 1H), 8.04–8.10 (m,

2H), 7.91 (dd, J = 8.72, 1.89 Hz, 1H), 7.64 (dd, J = 8.34, 4.29 Hz, 1H), 6.17 (s, 2H), 3.94 (s, 3H); HPLC purity (method B): RT 3.41, >95%.

Compounds **13**, **25**–**26**, and **28**–**33** were prepared according to general procedure B.

4-((6-(4-Fluorophenyl)-1H-[1,2,3]triazolo[4,5-b]pyrazin-1-yl)methyl)phenol (13). LC-MS m/z 322 (M + H)$^+$; ^{1}H NMR (400 MHz, DMSO-d_6) δ 9.5–9.57 (m, 1H), 9.48 (s, 1H), 8.36–8.44 (m, 2H), 7.47 (t, J = 8.72 Hz, 2H), 7.32 (d, J = 8.34 Hz, 2H), 6.74 (d, J = 8.34 Hz, 2H), 5.88 (s, 2H); HPLC purity (method B): RT 3.24, >95%.

6-(4-Fluorophenyl)-1-(4-methoxybenzyl)-1H-[1,2,3]triazolo-[4,5-b]pyrazine (25). LC-MS m/z 336 (M + H)$^+$; ^{1}H NMR (400 MHz, DMSO-d_6) δ 9.48 (s, 1H), 8.40 (dd, J = 5.43, 8.97 Hz, 2H), 7.39–7.51 (m, 4H), 6.93 (d, J = 8.59 Hz, 2H), 5.95 (s, 2H), 3.31 (s, 3H); HPLC purity (method A): RT 11.99, >99%.

1-(4-Fluorobenzyl)-6-(4-fluorophenyl)-1H-[1,2,3]triazolo[4,5-b]pyrazine (26). LC-MS m/z 324 (M + H)$^+$; ^{1}H NMR (400 MHz, DMSO-d_6) δ 9.49 (s, 1H), 8.38 (dd, J = 5.43, 8.97 Hz, 2H), 7.54 (dd, J = 5.56, 8.59 Hz, 2H), 7.46 (t, J = 8.84 Hz, 2H), 7.21 (t, J = 8.84 Hz, 2H), 6.02 (s, 2H); HPLC purity (method A): RT 11.59, >99%.

1-(4-Methoxybenzyl)-6-(1-methyl-1H-pyrazol-4-yl)-1H-[1,2,3]triazolo[4,5-b]pyrazine (28). LC-MS m/z 322 (M + H)$^+$; ^{1}H NMR (400 MHz, DMSO-d_6) δ 9.19 (s, 1H), 8.65 (s, 1H), 8.31 (s, 1H), 7.42 (d, J = 8.84 Hz, 2H), 6.93 (d, J = 8.84 Hz, 2H), 5.85 (s, 2H), 3.96 (s, 3H), 3.72 (s, 3H); HPLC purity (method A): RT 11.37, >99%.

1-((2,3-Dihydrobenzofuran-5-yl)methyl)-6-(1-methyl-1H-pyrazol-4-yl)-1H-[1,2,3]triazolo[4,5-b]pyrazine (29). LC-MS m/z 334 (M + H)$^+$; ^{1}H NMR (400 MHz, DMSO-d_6) δ 9.20 (s, 1H), 8.62–8.69 (m, 1H), 8.33 (s, 1H), 7.33 (s, 1H), 7.25 (d, J = 8.34 Hz, 1H), 6.75 (d, J = 8.08 Hz, 1H), 5.83 (s, 2H), 4.49 (t, J = 8.72 Hz, 2H), 3.97 (s, 3H), 3.13 (t, J = 8.72 Hz, 2H); HPLC purity (method B): RT 2.94, >95%.

1-((2,3-Dihydrobenzo[b][1,4]dioxin-6-yl)methyl)-6-(1-methyl-1H-pyrazol-4-yl)-1H-[1,2,3]triazolo[4,5-b]pyrazine (30). LC-MS m/z 350 (M + H)$^+$; ^{1}H NMR (400 MHz, DMSO-d_6) δ 9.17 (s, 1H), 8.63 (s, 1H), 8.29 (s, 1H), 6.96 (d, 1H), 6.89–6.92 (dd, 1H), 6.81–6.83 (d, 1H), 5.78 (s, 2H), 4.18 (s, 4H), 3.94 (s, 3H); HPLC purity (method A): RT 11.27, >99%.

6-((1-Methyl-1H-pyrazol-4-yl)-1H-[1,2,3]triazolo[4,5-b]-pyrazin-1-yl)methyl)quinoline (31). LC-MS m/z 343 (M + H)$^+$; ^{1}H NMR (400 MHz, DMSO-d_6) δ 9.22 (s, 1H), 8.90 (dd, J = 1.77, 4.29 Hz, 1H), 8.65 (s, 1H), 8.38 (dd, J = 1.01, 8.34 Hz, 1H), 8.31 (d, J = 0.51 Hz, 1H), 7.97–8.07 (m, 2H), 7.84 (dd, J = 2.02, 8.59 Hz, 1H), 7.54 (dd, J = 4.29, 8.34 Hz, 1H), 6.16 (s, 2H), 3.95 (s, 3H); HPLC purity (method A): RT 10.90, >99%.

6-((6-(1-Methyl-1H-pyrazol-4-yl)-1H-[1,2,3]triazolo[4,5-b]-pyrazin-1-yl)methyl)quinazoline (32). LC-MS m/z 344 (M + H)$^+$; ^{1}H NMR (400 MHz, DMSO-d_6) δ 9.60 (s, 1H), 9.28 (s, 1H), 9.21 (s, 1H), 8.62 (s, 1H), 8.29 (s, 1H), 8.08–8.15 (m, 2H), 8.00–8.06 (m, 1H), 6.19 (s, 2H), 3.93 (s, 3H); HPLC purity (method A): RT 10.58, >95%.

6-((6-(1H-pyrazol-4-yl)-1H-[1,2,3]triazolo[4,5-b]pyrazin-1-yl)methyl)quinoline (33). LC-MS m/z 329 (M + H)$^+$; ^{1}H NMR (400 MHz, DMSO-d_6) δ 13.47 (br s, 1H), 9.26 (s, 1H), 8.89 (dd, J = 4.17, 1.64 Hz, 1H), 8.55 (br s, 2H), 8.38 (d, J = 8.59 Hz, 1H), 7.99–8.07 (m, 2H), 7.84 (dd, J = 8.97, 1.64 Hz, 1H), 7.53 (dd, J = 8.34, 4.29 Hz, 1H), 6.15 (s, 2H); HPLC purity (method B): RT 2.38, >95%.

2-(4-(1-(Quinolin-6-ylmethyl)-1H-[1,2,3]triazolo[4,5-b]-pyrazin-6-yl)-1H-pyrazol-1-yl)ethanol (PF-04217903) (34). Step 1: 4-Iodo-1-(2-(tetrahydro-2H-pyran-2-yloxy)ethyl)-1H-pyrazole (58). In a round-bottom flask was added 4-iodopyrazole (10.22 g, 52.70 mmol), Cs$_2$CO$_3$ (20.6 g, 63.2 mmol), and anhydrous DMF (100 mL). The suspension was stirred at 23 °C for 5 min. 2-(2-Bromoethoxy)tetrahydro-2H-pyran (9.95 mL, 63.2 mmol) was added, and the reaction mixture was stirred at 70 °C for 16 h. After the reaction mixture was cooled down, EtOAc (100 mL) and water (100 mL) were added. The organic layer was collected, and the aqueous layer was extracted with EtOAc (3 × 100 mL). The combined organic layers were washed with water (3 × 100 mL), dried over Na$_2$SO$_4$, and concentrated to afford a dark brown oil. The crude product was purified on a silica gel column, eluting with ethyl acetate and hexanes

to provide **58** as a yellow oil (14.78 g, 87% yield). ^{1}H NMR (300 MHz, DMSO-d_6) δ 7.89 (s, 1H), 7.52 (s, 1H), 4.47–4.56 (m, 1H), 4.25–4.35 (m, 2H), 3.81–3.96 (m, 1H), 3.66–3.75 (m, 1H), 3.45–3.57 (m, 1H), 3.32–3.40 (m, 1H), 1.34–1.71 (m, 6H).

Step 2: 1-(2-(Tetrahydro-2H-pyran-2-yloxy)ethyl)-4-(4,4,5,5-tetramethyl-1,3,2-dioxaborolan-2-yl)-1H-pyrazole (60). To a solution of **57** (1.0 g, 3.1 mmol) in anhydrous THF (8 mL) was added i-PrMgCl (2 M in THF, 3.10 mL, 6.21 mmol) at 0 °C dropwise under nitrogen. The reaction was stirred for 1 h at 0 °C under nitrogen. To the solution was added 2-methoxy-4,4,5,5-tetramethyl-1,3,2-dioxaborolane (0.736 g, 4.66 mmol) at 0 °C, and the resulting yellow solution was allowed to stir for 1 h at ambient temperature under nitrogen. The reaction was quenched with a saturated aqueous solution of NH$_4$Cl (10 mL). EtOAc (50 mL) and saturated aqueous NH$_4$Cl solution (10 mL) were added. The organic layer was separated, and the aqueous layer was extracted with EtOAc (3 × 50 mL), dried over Na$_2$SO$_4$, and concentrated to give the crude product as a yellow oil. The oil was purified in a silica gel column, eluting with EtOAc and hexanes to provide **60** as clear oil (800 mg, 80% yield). ^{1}H NMR (300 MHz, DMSO-d_6) δ 7.91 (s, 1H), 4.48–4.54 (m, 1H), 4.26–4.33 (m, 2H), 3.86–3.90 (m, 1H), 3.66–3.76 (m, 1H), 3.45–3.57 (m, 1H), 3.33–3.39 (m, 1H), 1.33–1.70 (m, 6H), 1.24 (s, 12H).

Step 3: 6-((6-(1-(2-(Tetrahydro-2H-pyran-2-yloxy)ethyl)-1H-pyrazol-4-yl)-1H-[1,2,3]triazolo[4,5-b]pyrazin-1-yl)methyl)-quinoline (61). To a solution of **55d** (845 mg, 2.48 mmol) in DME (16 mL) was added **60** (800 mg, 2.48 mmol) and Cs$_2$CO$_3$ (2.42 g, 7.43 mmol) in H$_2$O (4 mL). The reaction mixture was degassed and charged with nitrogen three times. The palladium catalyst Pd(dppf)-Cl$_2$·CH$_2$Cl$_2$ (101 mg, 0.124 mmol) was added, and the reaction mixture was degassed and charged with nitrogen three times, and stirred for 16 h at 80 °C under nitrogen. The reaction mixture was then filtered over a pad of Celite and washed with EtOAc (50 mL) and water (25 mL). The filtrate was extracted with EtOAc (3 × 50 mL). The combined organic layers were dried over Na$_2$SO$_4$, filtered, and concentrated in vacuo. The crude product was purified via Biotage silica gel column chromatography, eluting with hexane/EtOAc (0–100%) to provide **61** (910 mg, 81% yield) as a white solid. ^{1}H NMR (300 MHz, DMSO-d_6) δ 9.23 (s, 1H), 8.82–8.95 (m, 1H), 8.67 (s, 1H), 8.28–8.45 (m, 2H), 7.92–8.08 (m, 2H), 7.77–7.90 (m, 1H), 7.53 (dd, J = 8.29, 4.14 Hz, 1H), 6.15 (s, 2H), 4.49–4.62 (m, 2H), 4.30–4.47 (m, 2H), 3.91–4.00 (m, 1H), 3.67–3.87 (m, J = 5.46 Hz, 1H), 3.47–3.60 (m, 1H), 3.35–3.42 (m, 1H), 1.48–1.66 (m, 2H), 1.32–1.45 (m, 3H).

Step 4: To a solution of **61** (780 mg, 1.71 mmol) in CH$_2$Cl$_2$ (20 mL) was added the anhydrous HCl/dioxane solution dropwise (4 N, 1.07 mL, 4.27 mmol). A white solid precipitated out. The reaction mixture was stirred for 1 h, and the LCMS showed the completion of the reaction. The reaction mixture was concentrated, and the residue was dissolved in distilled water (15 mL). The solution was adjusted to pH 7 with Na$_2$CO$_3$. An off-white solid crashed out, which was filtered, washed with water, and dried on a high vacuum for 1 h. The solid was recrystallized from EtOH (50 mL) to provide **2** (400 mg, 63% yield) as a white crystalline solid: mp 222 °C; LC-MS m/z 373 (M + H)$^+$; ^{1}H NMR (400 MHz, DMSO-d_6) δ 9.23 (s, 1H), 8.94 (dd, J = 1.52, 4.29 Hz, 1H), 8.64 (s, 1H), 8.46 (d, J = 8.59 Hz, 1H), 8.33 (s, 1H), 8.02–8.08 (m, 2H), 7.88 (dd, J = 1.89, 8.72 Hz, 1H), 7.59 (dd, J = 4.29, 8.34 Hz, 1H), 6.17 (s, 2H), 4.25 (t, J = 5.43 Hz, 2H), 3.79 (t, J = 5.43 Hz, 2H); HPLC purity (method A): RT 10.679, 99.6%; Anal. Calcd for C$_{19}$H$_{16}$N$_8$O·1.0H$_2$O: C, 58.45; H, 4.65; N, 28.70. Found: C, 58.45; H, 4.57; N, 28.50.

2-Methyl-1-(4-(1-(quinolin-6-ylmethyl)-1H-[1,2,3]triazolo-[4,5-b]pyrazin-6-yl)-1H-pyrazol-1-yl)propan-2-ol (36). To a suspension of **33** (50 mg, 0.15 mmol) and Cs$_2$CO$_3$ (50 mg, 0.15 mmol) in DMF (2 mL) was added 2,2-dimethyl-oxirane (21.6 mg, 0.30 mmol). The reaction was stirred at 80 °C for 16 h. The reaction was then purified with a reverse-phased preparative HPLC eluting with acetonitrile/water having 0.1% acetic acid to yield **36** as a white amorphous solid after lyophilization (13 mg, 22% yield); LC-MS m/z 401 (M + H)$^+$; ^{1}H NMR (400 MHz, DMSO-d_6) δ 9.25 (s, 1H), 8.90 (dd, J = 1.64, 4.17 Hz, 1H), 8.58 (s, 1H), 8.34–8.41 (m, 1H), 8.32 (s,

1H), 7.98−8.06 (m, 2H), 7.83 (dd, J = 2.02, 8.59 Hz, 1H), 7.54 (dd, J = 4.17, 8.21 Hz, 1H), 6.16 (s, 2H), 4.81 (s, 1H), 4.12 (s, 2H), 1.11 (s, 6H); HPLC purity (method A): RT 11.10, >99%.

N,N-Dimethyl-2-(4-(1-(quinolin-6-ylmethyl)-1H-[1,2,3]-triazolo[4,5-b]pyrazin-6-yl)-1H-pyrazol-1-yl)ethanamine (37). To a solution of **33** (50 mg, 0.152 mmol) in anhydrous DMF (1.52 mL, 0.1 M) was added cesium carbonate (100 mg, 0.304 mmol). The 1-(2-chloroethyl)pyrrolidine-HCl salt (26 mg, 0.152 mmol) was added, and the reaction mixture was allowed to stir under nitrogen for 3 h at 80 °C. The reaction mixture was purified directly by preparative HPLC using acetonitrile and H$_2$O with 0.1% HOAc to give **37** (15 mg, 23% yield); LC-MS m/z 400 (M + H)$^+$; ^{1}H NMR (400 MHz, DMSO-d$_6$) δ ppm 9.51 (br s, 1H), 9.27 (s, 1H), 8.93 (dd, J = 4.17, 1.64 Hz, 1H), 8.75−8.79 (m, 1H), 8.45−8.52 (m, 1H), 8.43 (d, J = 8.34 Hz, 1H), 8.05 (d, J = 8.59 Hz, 1H), 8.00 (d, J = 1.26 Hz, 1H), 7.85 (dd, J = 8.72, 1.89 Hz, 1H), 7.58 (dd, J = 8.21, 4.17 Hz, 1H), 6.17 (s, 2H), 4.64 (t, J = 6.19 Hz, 2H), 3.63 (br s, 2H), 2.83 (br s, 6H); HPLC purity (method A): RT 9.64, 95.30%.

38 and **39** were prepared with a similar procedure as that used for **37**.

6-((6-(1-(2-(Pyrrolidin-1-yl)ethyl)-1H-pyrazol-4-yl)-1H-[1,2,3]-triazolo[4,5-b]pyrazin-1-yl)methyl)quinoline (38). LC-MS m/z 426.1 (M + H)$^+$; ^{1}H NMR (400 MHz, DMSO-d$_6$) δ 9.20 (s, 1H), 8.88 (dd, J = 1.77, 4.29 Hz, 1H), 8.67 (s, 1H), 8.35−8.39 (m, 1H), 8.30 (s, 1H), 7.96−8.05 (m, 2H), 7.82 (dd, J = 2.02, 8.59 Hz, 1H), 7.51 (s, 1H), 6.14 (s, 2H), 4.30 (t, J = 6.44 Hz, 2H), 3.35−3.42 (m, 4H), 2.86 (t, J = 6.44 Hz, 2H), 2.44−2.48 (m, 4H), 1.63 (td, J = 3.22, 6.69 Hz, 4H); HPLC purity (method A): RT 9.86, >99%.

1-(2-(4-(1-(Quinolin-6-ylmethyl)-1H-[1,2,3]triazolo[4,5-b]-pyrazin-6-yl)-1H-pyrazol-1-yl)ethyl)pyrrolidin-2-one (39). LC-MS m/z 440.0 (M + H)$^+$; ^{1}H NMR (400 MHz, DMSO-d$_6$) δ 9.23 (s, 1H), 8.90 (dd, J = 1.77, 4.04 Hz, 1H), 8.69 (s, 1H), 8.38 (d, J = 7.33 Hz, 1H), 8.34 (s, 1H), 7.99−8.06 (m, 2H), 7.84 (dd, J = 2.02, 8.84 Hz, 1H), 7.54 (dd, J = 4.29, 8.34 Hz, 1H), 6.16 (s, 2H), 4.34 (t, J = 5.94 Hz, 2H), 3.62 (t, J = 5.94 Hz, 2H), 3.10−3.20 (m, 2H), 2.07−2.17 (m, 2H), 1.82 (t, J = 7.45 Hz, 2H); HPLC purity (method A): RT 10.79, >99%.

2-(4-(1-(Quinolin-6-ylmethyl)-1H-[1,2,3]triazolo[4,5-b]-pyrazin-6-yl)-1H-pyrazol-1-yl)acetic acid (35). The methyl ester of **35** was prepared with a similar procedure as that used for **37**. To a solution of 2-(4-(1-(quinolin-6-ylmethyl)-1H-[1,2,3]triazolo[4,5-b]-pyrazin-6-yl)-1H-pyrazol-1-yl)acetic acid methyl ester (242 mg, 0.60 mmol) in MeOH (4 mL) was added a freshly prepared solution of LiOH (72 mg, 3.02 mmol) in water (1 mL). The reaction was stirred for 16 h at ambient temperature. The white suspension was then neutralized to pH 7 with 1 N HCl, and a white solid precipitated out. The solid was filtered, washed with water, and dried under a high vacuum for 16 h to provide **35** (131 mgs, 56% yield); LC-MS m/z 387 (M + H)$^+$; ^{1}H NMR (400 MHz, DMSO-d$_6$) δ 9.15 (s, 1H), 8.82 (d, J = 2.78 Hz, 1H), 8.52 (s, 1H), 8.31 (d, J = 7.58 Hz, 1H), 8.19 (s, 1H), 7.90−8.00 (m, 2H), 7.78 (s, 1H), 7.42−7.50 (m, 1H), 6.09 (s, 2H), 4.54−4.69 (m, 2H); HPLC purity (method A): RT 10.21, 96.19%.

(R)-6-((6-(1-(Pyrrolidin-3-yl)-1H-pyrazol-4-yl)-1H-[1,2,3]-triazolo[4,5-b]pyrazin-1-yl)methyl)quinoline (40). The N-Boc analogue of **40** was prepared according to a similar procedure as that used for **37**. The Boc-protecting group was removed with 4 N HCl in dioxane in methanol solvent; LC-MS m/z 398 (M + H)$^+$; ^{1}H NMR (400 MHz, DMSO-d$_6$) δ 9.26 (s, 1H), 9.16 (br s, 2H), 8.94 (dd, J = 2.78, 1.52 Hz, 1H), 8.82 (s, 1H), 8.44 (s, 2H), 8.00−8.10 (m, 2H), 7.86 (d, J = 8.84 Hz, 1H), 7.59 (ddd, J = 6.19, 4.17, 2.02 Hz, 1H), 6.17 (s, 2H), 5.26−5.38 (m, J = 7.14, 7.14, 4.04, 3.66 Hz, 1H), 3.65−3.74 (m, 1H), 3.57−3.65 (m, 1H), 3.44 (d, J = 16.67 Hz, 2H), 2.41−2.48 (m, 1H), 2.29−2.40 (m, 1H); HPLC purity (method A): RT 9.90, 99%.

6-((6-(1-(Piperidin-4-yl)-1H-pyrazol-4-yl)-1H-[1,2,3]triazolo-[4,5-b]pyrazin-1-yl)methyl)quinoline (41). The N-Boc analogue of **41** was prepared according to a similar procedure as that used for **37**. The Boc-protecting group was removed with 4 N HCl in dioxane in methanol solvent; LC-MS m/z 412 (M + H)$^+$; ^{1}H NMR (400 MHz, DMSO-d$_6$, 2 equiv HCl-salt) δ 9.27 (s, 1H), 8.84−8.98 (m, 2H),

8.62−8.76 (m, 2H), 8.48 (d, J = 7.58 Hz, 1H), 8.37 (s, 1H), 8.01−8.10 (m, 2H), 7.88 (d, J = 8.59 Hz, 1H), 7.61 (dd, J = 4.29, 8.08 Hz, 1H), 6.17 (s, 2H), 4.61 (t, J = 10.74 Hz, 1H), 3.36−3.46 (m, J = 12.60 Hz, 2H), 3.01−3.19 (m, 2H), 2.10−2.29 (m, 4H); HPLC purity (method A): RT 10.00, >99%.

6-((1H-[1,2,3]Triazolo[4,5-b]pyrazin-1-yl)methyl)quinoline (42). A solution of **55d** (200 mg, 0.586 mmol) in MeOH (10 mL)/AcOH (1 mL)/EtOAc (1 mL) was degassed 3 times with nitrogen. To this solution was added Pd/C (20 mg). A balloon containing hydrogen was added via syringe, and the reaction was allowed to stir for 18 h at room temperature. The reaction did not complete, and more Pd/C was added (20 mg) and stirred for 18 h at room temperature. The reaction was stopped when LCMS showed a ratio of 1:1 (product/starting material). The reaction was filtered over Celite and washed with EtOAc (50 mL). The filtered solution was concentrated and purified by Biotage silica gel column chromatography with hexane/EtOAc to give **42** as a white solid (30 mg, 20% yield); LC-MS m/z 263.0 (M + H)$^+$; ^{1}H NMR (400 MHz, DMSO-d$_6$) δ 8.85−8.92 (m, 3H), 8.31−8.39 (m, 1H), 8.00 (d, J = 8.59 Hz, 1H), 7.96 (d, J = 1.52 Hz, 1H), 7.77 (dd, J = 2.15, 8.72 Hz, 1H), 7.52 (dd, J = 4.17, 8.21 Hz, 1H), 6.22 (s, 2H); HPLC purity (method A): RT 10.11, 97.2%.

6-((6-Methyl-1H-[1,2,3]triazolo[4,5-b]pyrazin-1-yl)methyl)-quinoline (43). To a solution of **55d** (100 mg, 0.29 mmol) and methyl boronic acid (20 mg, 0.32 mmol) in DME/H$_2$O (4:1, 0.1 M) was added sodium carbonate (92 mg, 0.87 mmol). The mixture was degassed with nitrogen three times. Pd(PPh$_3$)$_2$Cl$_2$ (10 mg, 0.015 mmol) was added, and the reaction was degassed again three times. After it was heated to 80 °C for 16 h, the reaction mixture was filtered through a pad of Celite and washed with EtOAc. The aqueous layer was extracted with EtOAc (3 × 10 mL), dried over Na$_2$SO$_4$, filtered, and concentrated in vacuo. The crude material was purified directly by preparative HPLC using ACN/H$_2$O with 0.1% HOAc to afford **43** (13 mg, 16%); LC-MS m/z 277.1 (M + H)$^+$; ^{1}H NMR (400 MHz, DMSO-d$_6$) δ 8.90 (dd, J = 1.77, 4.29 Hz, 1H), 8.79 (s, 1H), 8.36 (d, J = 7.58 Hz, 1H), 8.01 (d, J = 8.84 Hz, 1H), 7.91 (s, 1H), 7.75 (dd, J = 2.02, 8.59 Hz, 1H), 7.53 (dd, J = 4.29, 8.34 Hz, 1H), 6.17 (s, 2H), 2.74 (s, 3H); HPLC purity (method B): RT 2.60, 95%.

1-(Quinolin-6-ylmethyl)-1H-[1,2,3]triazolo[4,5-b]pyrazin-6-amine (44). To a microwave vessel were added **55d** (300 mg, 0.88 mmol) and NH$_4$OH (3 mL). The reaction was irradiated in a microwave at 100 °C for 1 h. The solid was filtered and washed with water and then recrystallized in MeOH, filtered, and dried to give **44** as a white crystal solid (100 mg, 41%); mp 266 °C; LC-MS m/z 278 (M + H)$^+$; ^{1}H NMR (400 MHz, DMSO-d$_6$) δ 8.89 (dd, J = 1.64, 4.17 Hz, 1H), 8.35 (dd, J = 1.01, 8.34 Hz, 1H), 8.04 (s, 1H), 7.99−8.03 (m, 1H), 7.80 (d, J = 1.52 Hz, 1H), 7.68 (dd, J = 2.02, 8.84 Hz, 1H), 7.49−7.56 (m, 3H), 5.88 (s, 2H); HPLC purity (method A): RT 9.33, >99%.

(R)-1-(1-(Quinolin-6-ylmethyl)-1H-[1,2,3]triazolo[4,5-b]-pyrazin-6-yl)pyrrolidin-3-amine (48). Step 1. A mixture of **55d** (200 mg, 0.59 mmol), potassium carbonate (243 mg, 1.76 mmol), and (R)-tertbutylpyrrolidin-3-ylcarbamate (218 mg, 1.17 mmol) in 2-propanol (6 mL) was heated in the microwave at 80 °C for 20 min. The mixture was allowed to cool, and the solids were collected by filtration and then purified by flash chromatography, eluting with chloroform/ethyl acetate (25−75%) to afford the N-Boc protected **48** (239 mg, 91%).

Step 2. To a solution of (R)-tert-butyl 1-(1-(quinolin-6-ylmethyl)-1H-[1,2,3]triazolo[4,5-b]pyrazin-6-yl)pyrrolidin-3-ylcarbamate (100 mg, 0.224 mmol) in dichloromethane (2.2 mL) was added hydrochloric acid (4 N in dioxane 0.56 mL, 2.24 mmol). After stirring at room temperature for 6 h, the reaction was diluted with dichloromethane and quenched with saturated sodium bicarbonate (5 mL). The organic layer was separated and concentrated to afford the desired product **48** (65 mg, 84%); LC-MS m/z 347 (M + H)$^+$; ^{1}H NMR (400 MHz, methanol-d$_4$) δ 8.85 (dd, J = 1.5, 4.3 Hz, 1H), 8.36 (d, J = 8.3 Hz, 1H), 8.15 (s, 1H), 8.01 (d, J = 8.6 Hz, 1H), 7.95 (d, J = 1.0 Hz, 1H), 7.85 (dd, J = 2.0, 8.8 Hz, 1H), 7.55 (dd, J = 4.4, 8.5 Hz, 1H), 5.95 (s, 2H), 3.88−3.78 (m, 2H), 3.75−3.66 (m, 2H), 3.48−3.40

(m, 1H), 2.35–2.22 (m, 1H), 2.03–1.86 (m, 1H); HPLC purity (method A): RT 8.96, >99%.

Compounds **45–47** and **49–50** were prepared with similar procedures as that for **48**.

***N*-Ethyl-1-(quinolin-6-ylmethyl)-1*H*-[1,2,3]triazolo[4,5-*b*]-pyrazin-6-amine (45).** LC-MS *m/z* 306 (M + H)$^+$; ^{1}H NMR (400 MHz, DMSO-*d*$_6$) δ 8.88 (dd, *J* = 1.64, 4.17 Hz, 1H), 8.32–8.38 (m, 1H), 8.19 (br s, 1H), 7.96–8.04 (m, 2H), 7.89–7.94 (m, 1H), 7.74 (dd, *J* = 2.02, 8.84 Hz, 1H), 7.53 (dd, *J* = 4.29, 8.34 Hz, 1H), 5.87 (s, 2H), 3.34–3.39 (m, 2H), 1.16 (t, *J* = 7.20 Hz, 3H); HPLC purity (method A): RT 11.13, >99%.

2-(1-(Quinolin-6-ylmethyl)-1*H*-[1,2,3]triazolo[4,5-*b*]pyrazin-6-ylamino)ethanol (46). LC-MS *m/z* 322 (M + H)$^+$; ^{1}H NMR (400 MHz, DMSO-*d*$_6$) δ 8.89 (dd, *J* = 1.6, 4.2 Hz, 1H), 8.36 (d, *J* = 8.3 Hz, 1H), 8.26 (t, *J* = 5.8 Hz, 1H), 8.10 (s, 1H), 8.00 (d, *J* = 8.6 Hz, 1H), 7.93 (d, *J* = 1.3 Hz, 1H), 7.76 (dd, *J* = 2.0, 8.6 Hz, 1H), 7.53 (dd, *J* = 4.3, 8.3 Hz, 1H), 5.87 (s, 2H), 4.82 (t, *J* = 5.3 Hz, 1H), 3.58 (q, *J* = 5.6 Hz, 2H), 3.44 (q, *J* = 5.7 Hz, 2H); HPLC purity (method A): RT 10.20, >99%.

N^1,N^1-Dimethyl-N^2-(1-(quinolin-6-ylmethyl)-1*H*-[1,2,3]-triazolo[4,5-*b*]pyrazin-6-yl)ethane-1,2-diamine (47). LC-MS *m/z* 349 (M + H)$^+$; ^{1}H NMR (400 MHz, methanol-*d*$_4$) δ 8.83 (dd, *J* = 1.52, 4.29 Hz, 1H), 8.34 (d, *J* = 8.08 Hz, 1H), 7.96–8.05 (m, 2H), 7.92 (s, 1H), 7.79 (dd, *J* = 2.02, 8.84 Hz, 1H), 7.53 (dd, *J* = 4.29, 8.34 Hz, 1H), 5.93 (s, 2H), 3.59 (t, *J* = 6.57 Hz, 2H), 2.59 (t, *J* = 6.57 Hz, 2H), 2.24 (s, 6H); HPLC purity (method A): RT 8.34, >99%.

1-(1-(Quinolin-6-ylmethyl)-1*H*-[1,2,3]triazolo[4,5-*b*]pyrazin-6-yl)pyrrolidin-3-ol (49). LC-MS *m/z* 348 (M + H)$^+$; ^{1}H NMR (400 MHz, DMSO-*d*$_6$) δ 8.89 (dd, *J* = 1.77, 4.04 Hz, 1H), 8.36 (d, *J* = 7.58 Hz, 1H), 8.22 (s, 1H), 8.00 (d, *J* = 8.59 Hz, 1H), 7.90–7.96 (m, 1H), 7.76 (dd, *J* = 1.89, 8.72 Hz, 1H), 7.53 (dd, *J* = 4.17, 8.21 Hz, 1H), 5.90 (s, 2H), 5.10 (br s, 1H), 4.43 (br s, 1H), 3.56–3.80 (m, 3H), 3.48–3.55 (m, 1H), 1.84–2.08 (m, 2H); HPLC purity (method A): RT 10.01, >99%.

6-((6-(4-Methylpiperazin-1-yl)-1*H*-[1,2,3]triazolo[4,5-*b*]-pyrazin-1-yl)methyl)quinoline (50). LC-MS *m/z* 361 (M + H)$^+$; ^{1}H NMR (400 MHz, chloroform-*d*) δ 8.92 (br s, 1H), 8.30 (s, 1 H), 8.12 (d, *J* = 8.3 Hz, 1H), 8.08 (d, *J* = 8.8 Hz, 1H), 7.82 (s, 1 H), 7.77 (dd, *J* = 1.9, 8.7 Hz, 1H), 7.41 (dd, *J* = 4.3, 8.3 Hz, 1H), 5.88 (s, 2H), 3.86–3.78 (m, 4H), 2.59 (br s, 4H), 2.39 (s, 3H); HPLC purity (method A): RT 8.45, >99%.

***N*,*N*-Dimethyl-2-(1-(quinolin-6-ylmethyl)-1*H*-[1,2,3]triazolo-[4,5-*b*]pyrazin-6-yloxy)ethanamine (51).** A mixture of **55d** (100 mg, 0.293 mmol), triethylamine (0.123 mL, 0.879 mmol), and *N*,*N*-dimethylethanolamine (0.959 mL, 0.586 mmol) in *n*-butanol (3.0 mL) was heated in the microwave at 120 °C for 20 min and then concentrated. The crude product was purified by flash chromatography using a Horizon purification system on a 25S column eluting with chloroform/7 N ammonia in methanol (0.1–5%) to afford **49** (75 mg, 74%); LC-MS *m/z* 350 (M + H)$^+$; ^{1}H NMR (400 MHz, DMSO-*d*$_6$) δ 8.89 (dd, *J* = 1.6, 4.2 Hz, 1H), 8.42 (s, 1H), 8.36 (d, *J* = 7.6 Hz, 1H), 8.01 (d, *J* = 8.6 Hz, 1H), 7.97 (d, *J* = 1.5 Hz, 1H), 7.78 (dd, *J* = 2.0, 8.8 Hz, 1H), 7.53 (dd, *J* = 4.3, 8.3 Hz, 1H), 6.06 (s, 2H), 4.50 (t, *J* = 5.7 Hz, 2H), 2.61 (t, *J* = 5.7 Hz, 2H), 2.13 (s, 6H); HPLC purity (method A): RT 8.09, 99%.

Biochemical Kinase Assays. c-MET enzyme inhibition was measured by a continuous coupled spectrophotometric assay as previously described.[23] The assay monitored ATP consumption coupled to oxidation of NADH (measured at 340 nm) while regenerating ATP in the presence of phosphoenol pyruvate (PEP) and coupling enzymes, pyruvate kinase (PK), and lactic dehydrogenase (LDH). Assay reactions contained 0.30 mM ATP ($4K_m$), 0.5 mM Met2 peptide (Ac-ARDMYDKEYYSVHNK), 20 mM MgCl$_2$, 1 mM PEP, 330 μM NADH, 2 mM DTT, 15 units/mL LDH, 15 units/mL PK, test compound (1% DMSO final) in 100 mM HEPES, pH 7.5, 37 °C, and the reactions were initiated by adding 50 nM c-Met N-terminal His6-tagged recombinant human enzyme, aa residues 974–1390 (Millipore Corp./Upstate Ltd., Billerica, MA). The inhibitors were shown to be ATP-competitive from kinetic and crystallographic studies, and the dose–response data were fit to the equation for

competitive inhibition by the method of nonlinear least-squares (GraphPad Prism, GraphPad Software, San Diego, CA).

Cellular Kinase Phosphorylation ELISA Assays.[36,32] All experiments were done under standard conditions (37 °C and 5% CO$_2$). IC50 values were calculated by concentration–response curve fitting using a Microsoft Excel-based four-parameter method. Cells were seeded in 96-well plates in media supplemented with 10% fetal bovine serum (FBS) and transferred to serum-free media [with 0.04% bovine serum albumin (BSA)] after 24 h. In experiments investigating ligand-dependent RTK phosphorylation, corresponding growth factors were added for up to 20 min. After incubation of cells with an inhibitor for 1 h and/or appropriate ligands for the designated times, cells were washed once with HBSS supplemented with 1 mmol/L Na$_3$VO$_4$, and protein lysates were generated from cells. Subsequently, phosphorylation of selected protein kinases was assessed by a sandwich ELISA method using specific capture antibodies used to coat 96-well plates and a detection antibody specific for phosphorylated tyrosine residues. Antibody-coated plates were (a) incubated in the presence of protein lysates at 4 °C overnight; (b) washed seven times in 1% Tween 20 in PBS; (c) incubated in a horseradish peroxidase-conjugated anti-total-phosphotyrosine (PY-20) antibody (1:500) for 30 min; (d) washed seven times again; (e) incubated in 3,3,5,5-tetramethylbenzidine peroxidase substrate (Bio-Rad) to initiate a colorimetric reaction that was stopped by adding 0.09 N H$_2$SO$_4$; and (f) measured for absorbance in 450 nm using a spectrophotometer. The A549 cell line was used for the c-MET cellular kinase phosphorylation ELISA assay.

Human Microsomal Stability Studies. Compounds (1 μM) were incubated at 37 °C for 30 min in a final volume of 200 μL of 100 mM potassium phosphate buffer (pH 7.4) containing pooled human liver microsomes (0.8 mg/mL protein) and 2 mM NADPH. Reactions were initiated with the addition of NADPH following a 10-min preincubation. Aliquots of incubation samples were protein precipitated with cold methanol containing 0.1 μM buspirone (internal standard) and centrifuged, and supernatants were analyzed by LC-MS/MS. All incubations were performed in triplicate, and the percent remaining of parent drug at the end of incubation was determined by LC-MS/MS peak area ratio.

Cocrystal Structures. c-MET cocrystals were obtained at 13 °C by the hanging drop vapor diffusion method by mixing 1.2 μL of protein solution (containing 7–13 mg/mL c-MET KD (residues 1051–1348) with a 5-fold molar excess of selected c-MET inhibitor) with 1.2 μL of solution containing 0.05 M citrate-phosphate pH 4.6, 0–0.275 M NaCl, and 21% polyethylene glycol MW = 3350. Details of the crystal structure determinations can be accessed from the PDB database.

■ ASSOCIATED CONTENT

ⓈSupporting Information

Kinase selectivity screening data for **12** against a total of 98 protein kinases. This material is available free of charge via the internet at http://pubs.acs.org.

Accession Codes

Coordinates of the c-MET crystal structures have been deposited in the Protein Data Bank for compounds **2** (3zxz), **10** (3zze), **12** (4ap7), and **24** (4aoi).

■ AUTHOR INFORMATION

Corresponding Author

*Phone: 858-638-6333. Fax: 877-481-1783. E-mail: jean.cui@pfizer.com.

Present Address

§Groton Laboratories, Pfizer Worldwide Research and Development, Eastern Point Road, Groton, Connecticut 06340.

Notes

The authors declare no competing financial interest.

■ ABBREVIATIONS

A-loop, activation loop; HGF, hepatocyte growth factor; HGFR, hepatocyte growth factor receptor; KD, kinase domain; c-MET, mesenchymal-epithelial transition factor; OS, overall survival; PFS, progression free survival; RTK, receptor tyrosine kinase; TKI, tyrosine kinase inhibitor

■ REFERENCES

(1) (a) Comoglio, P. M.; Tamagnone, L.; Boccaccio, C. Plasminogen-related growth factor and semaphorin receptors: a gene superfamily controlling invasive growth. *Exp. Cell Res.* **1999**, *253*, 88–99. (b) Comoglio, P. M.; Trusolino, L. Invasive growth: from development to metastasis. *J. Clin. Invest.* **2002**, *109*, 857–862.

(2) (a) Maulik, G.; Shrikhande, A.; Kijima, T.; Ma, P. C.; Morrison, P. T.; Salgia, R. Role of the hepatocyte growth factor receptor, c-MET, in oncogenesis and potential for therapeutic inhibition. *Cytokine Growth Factor Rev.* **2002**, *13*, 41–59. (b) Ma, P. C.; Maulik, G.; Christensen, J.; Salgia, R. c-MET: structure, functions and potential for therapeutic inhibition. *Cancer Metastasis Rev.* **2003**, *22*, 309–325. (c) Christensen, J.; Burrows, J.; Salgia, R. c-MET as a target in human cancer and characterization of inhibitors for therapeutic intervention. *Cancer Lett. (Amsterdam, Neth.)* **2005**, *225*, 1–26. (d) Benvenuti, S.; Comoglio, P. M. The met receptor tyrosine kinase in invasion and metastasis. *J. Cell. Physiol.* **2007**, *213*, 316–325. (e) Knudsen, B. S.; Vande Woude, G. Showering c-MET-dependent cancers with drugs. *Curr. Opin. Genet. Dev.* **2008**, *18*, 87–96.

(3) (a) Cheng, H.-L.; Trink, B.; Tzai, T.-S.; Liu, H.-S.; Chan, S.-H.; Ho, C.-L.; Sidransky, D.; Chow, N.-H. Overexpression of c-MET as a prognostic indicator for transitional cell carcinoma of the urinary bladder: a comparison with p53 nuclear accumulation. *J. Clin. Oncol.* **2002**, *20*, 1544–1550. (b) Lengyel, E.; Prechtel, D.; Resau, J. H.; Gauger, K.; Welk, A.; Lindemann, K.; Alanti, G.; Richter, T.; Knudsen, B.; Vande Woude, G. F.; Harneck, N. c-MET overexpression in node-positive breast cancer identifies patients with poor clinical outcome independent of Her2/neu. *Int. J. Cancer* **2005**, *113*, 678–682. (c) Lo Muzio, L.; Farina, A.; Rubini, C.; Coccia, E.; Capogreco, M.; Colella, G.; Leonardi, R.; Campisi, G.; Carinci, F. Effect of c-MET expression on survival in head and neck squamous cell carcinoma. *Tumor Biol.* **2006**, *27*, 116–121. (d) Sawada, K.; Radjabi, A. E.; Shinomiya, N.; Kistner, E.; Kenny, H.; Becker, A. R.; Turkyilmaz, M. A.; Salgia, R.; Yamada, S. D.; Vande Woude, G. F.; Tretiakova, M. S.; Lengyel, E. c-MET overexpression is a prognostic factor in ovarian cancer and an effective target for inhibition of peritoneal dissemination and invasion. *Cancer Res.* **2007**, *67*, 1670–1679. (e) Drebber, U.; Baldus, S. E.; Nolden, B.; Grass, G.; Bollschweiler, E.; Dienes, H. P.; Hölscher, A. H.; Mönig, S. P. Overexpression of c-MET as a prognostic indicator for gastric carcinoma compared to p53 and p21 nuclear accumulation. *Oncol. Rep.* **2008**, *19*, 1477–1483.

(4) (a) Matsumoto, K.; Nakamura, T. Mechanism and significance of bifunctional NK4 in cancer treatment. *Biochem. Biophys. Res. Commun.* **2005**, *333*, 316–327. (b) Otsuka, T.; Jakubczak, J.; Vieira, W.; Bottaro, D. P.; Breckenridge, D.; Larochelle, W. J.; Merlino, G. Disassociation of met-mediated biological responses in vivo: the natural hepatocyte growth factor/scatter factor splice variant NK2 antagonizes growth but facilitates metastasis. *Mol. Cell. Biol.* **2000**, *20*, 2055–2065. (c) Matsumoto, K; Nakamura, T.; Sakai, K.; Nakamura, T. Hepatocyte growth factor and Met in tumor biology and therapeutic applications with NK4. *Proteomics* **2008**, *8*, 3360–3370.

(5) Burgess, T.; Coxon, A.; Meyer, S.; Sun, J.; Rex, K.; Tsuruda, T.; Chen, Q.; Ho, S.-Y.; Li, L.; Kaufman, S.; McDorman, K.; Cattley, R. C.; Sun, J.; Elliott, G.; Zhang, K.; Feng, X.; Jia, X.-C.; Green, L.;

Radinsky, R.; Kendall, R. Fully human monoclonal antibodies to hepatocyte growth factor with therapeutic potential against hepatocyte growth factor/c-Met-dependent human tumors. *Cancer Res.* **2006**, *66*, 1721–1729.

(6) (a) Jin, H.; Yang, R.; Zheng, Z.; Romero, M.; Ross, J.; Bou-Reslan, H.; Carano, R.A.D.; Kasman, I.; Mai, E.; Young, J.; Zha, J.; Zhang, Z.; Ross, S.; Schwall, R.; Colbern, G.; Merchant, M. MetMAb, the one-armed 5D5 anti-c-Met antibody, inhibits orthotopic pancreatic tumor growth and improves survival. *Cancer Res.* **2008**, *68*, 4360–4368. (b) van der Horst, E. H.; Chinn, L.; Wang, M.; Velilla, T.; Tran, H.; Madrona, Y.; Lam, A.; Ji, M.; Hoey, T. C.; Sato, A. K. Discovery of fully human anti-MET monoclonal antibodies with antitumor activity against colon cancer tumor models *in vivo*. *Neoplasia* **2009**, *11*, 355–364.

(7) Liu, X.; Newton, R. C.; Scherle, P. A. Development of c-MET pathway inhibitors. *Expert Opin. Invest. Drugs* **2011**, *20*, 1225–1241.

(8) Tuma, R. S. Novel antibody, rilotumumab (AMG 102) shows activity in metastatic colorectal cancer patients. *Oncology Times* **2011**, *33*, 22–23.

(9) (a) Catenacci, D. V. T.; Henderson, L.; Xiao, S.-Y.; Patel, P.; Yauch, R. L.; Hegde, P.; Zha, J.; Pandita, A.; Peterson, A.; Salgia, R. Durable complete response of metastatic gastric cancer with anti-Met therapy followed by resistance at recurrence. *Cancer Discovery* **2011**, *1*, 573–579. (b) Surati, M.; Patel, P.; Peterson, A.; Salgia, R. Role of MetMAb (OA-5D5) in c-MET active lung malignancies. *Expert Opin. Biol. Ther.* **2011**, *11*, 1655–1662.

(10) Spigel, D. R.; Ervin, T. J.; Ramlau, R.; Daniel, D. B.; Goldschmidt, J. H.; Blumenschein, G. R.; Krzakowski, M. J.; Robinet, G.; Clement-Duchene, C.; Barlesi, F.; Govindan, R.; Patel, T.; Orlov, S. V.; Wertheim, M. S.; Zha, J.; Pandita, A.; Yu, W.; Yauch, R. L.; Patel, P. H.; Peterson, A. C. Final efficacy results from OAM4558g, a randomized phase II study evaluating MetMAb or placebo in combination with erlotinib in advanced NSCLC. Presented at ASCO 2011 Annual Meeting, Chicago, IL, June 3–7, 2011; Abstr. 7505.

(11) (a) Mroczkowski, B.; McTigue, M. A.; Sarup, J.; Murray, B. W.; Hickey, M.; Parge, H.; Zhu. J. Catalytic domains of the human hepatocyte growth factor receptor kinase and material and methods for identification thereof. USP 277968, EP1243596A1, 2001. (b) Schiering, N.; Knapp, S.; Marconi, M.; Flocco, M. M.; Cui, J.; Perego, R.; Rusconi, L.; Cristiani, C. Crystal structure of the tyrosine kinase domain of the hepatocyte growth factor receptor c-MET and its complex with the microbial alkaloid K-252a. *Proc. Natl. Acad. Sci. U.S.A.* **2003**, *100*, 12654–12659.

(12) Qian, F.; Engst, S.; Yamaguchi, K.; Yu, P.; Won, K.-A.; Mock, L.; Tracy Lou, T.; Tan, J.; Li, C.; Tam, D.; Lougheed, J.; Yakes, F. M.; Bentzien, F.; Xu, W.; Zaks, T.; Wooster, R.; Greshock, J.; Joly, A. H. Inhibition of tumor cell growth, invasion, and metastasis by EXEL-2880 (XL880, GSK1363089), a novel inhibitor of HGF and VEGF receptor tyrosine kinases. *Cancer Res.* **2009**, *69*, 8009–8016.

(13) Srinivasan, R.; Choueiri, T. K.; Vaishampayan, U.; Rosenberg, J. E.; Stein, M. N.; Logan, T.; Bukowski, R. M.; Mueller, T.; Keer, H. N.; Linehan, W. M. A phase II study of the dual MET/VEGFR2 inhibitor XL880 in patients (pts) with papillary renal carcinoma (PRC). Presented at ASCO 2008 Annual Meeting, Chicago, IL, May 30–June 3, 2008; Abstr. 5103.

(14) Jhawer, M. P.; Kindler, H. L.; Wainberg, Z. A.; Hecht, J. R.; Kerr, R. O.; Ford, J. M.; Henderson, C.; Mueller, T.; Keer, H. N.; Shah, M. A. Preliminary activity of XL880, a dual MET/VEGFR2 inhibitor, in MET amplified poorly differentiated gastric cancer (PDGC): Interim results of a multicenter phase II study. Presented at ASCO 2008 Annual Meeting, Chicago, IL, May 30–June 3, 2008; Abstr. 4572.

(15) (a) Katz, J. D.; Jewell, J. P.; Guerin, D. J.; Lim, J.; Dinsmore, C. J.; Deshmukh, S. V.; Pan, B.-S.; Marshall, C. G.; Lu, W.; Altman, M. D.; Dahlberg, W. K.; Davis, L.; Falcone, D.; Gabarda, A. E.; Hang, G.; Hatch, H.; Holmes, R.; Kunii, K.; Lumb, K. J.; Lutterbach, B.; Mathvink, R.; Nazef, N.; Patel, S. B.; Qu, X.; Reilly, J. F.; Rickert, K. W.; Rosenstein, C.; Soisson, S. M.; Spencer, K. B.; Szewczak, A. A.;

Walker, D.; Wang, W.; Young, J.; Zeng, Q. Discovery of a 5*H*-benzo[4,5]cyclohepta[1,2-b]pyridin-5-one (MK-2461) inhibitor of c-Met kinase for the treatment of cancer. *J. Med. Chem.* **2011**, *54*, 4092−4108. (b) Rickert, K. W.; Patel, S. B.; Allison, T. J.; Byrne, N. J.; Darke, P. L.; Ford, R. E.; Guerin, D. J.; Hall, D. L.; Kornienko, M.; Lu, J.; Munshi, S. K.; Reid, J. C.; Shipman, J. M.; Stanton, E. F.; Wilson, K. J.; Young, J. R.; Soisson, S. M.; Lumb, K. J. Structural basis for selective small molecule kinase inhibition of activated c-Met. *J. Biol. Chem.* **2011**, *286*, 11218−11225.

(16) Cui, J. J.; Tran-Dubé, M.; Shen, H.; Nambu, M.; Kung, P. P.; Pairish, M.; Jia, L.; Meng, J.; Funk, L.; Botrous, I.; McTigue, M.; Grodsky, N.; Ryan, K.; Padrique, E.; Alton, G.; Timofeevski, S.; Yamazaki, S.; Li, Q.; Zou, H.; Christensen, J.; Mroczkowski, B.; Bender, S.; Kania, R. S.; Edwards, M. P. Structure based drug design of crizotinib (PF-02341066), a potent and selective dual inhibitor of mesenchymal-epithelial transition factor (c-MET) kinase and anaplastic lymphoma kinase (ALK). *J. Med. Chem.* **2011**, *54*, 6342−6363.

(17) Kwak, E. L.; Bang, Y.-J.; Camidge, R.; Shaw, A. T.; Solomon, B; Maki, R. G.; Ou, S.-H. I.; Dezube, B. J.; Jänne, P. A.; Costa, D. B.; Varella-Garcia, M.; Kim, W.-H.; Lynch, T. J.; Fidias, P.; Stubbs, H.; Engelman, J. A.; Sequist, L. V.; Tan, W.; Gandhi, L.; Mino-Kenudson, M.; Wei, G. C.; Shreeve, S. M.; Ratain, M. J.; Settleman, J.; Christensen, J. G.; Haber, D. A.; Wilner, K.; Salgia, R.; Shapiro, G. I.; Clark, J. W.; Iafrate, A. J. Anaplastic lymphoma kinase inhibition in non-small-cell-lung cancer. *N. Engl. J. Med.* **2010**, *363*, 1693−1703.

(18) Ou, S.-H. I.; Kwak, E. L.; Siwak-Tapp, C.; Dy, J.; Bergethon, K.; Clark, J. W.; Camidge, D. R.; Solomon, B. J.; Maki, R. G.; Bang, Y.-J.; Kim, D.-W.; Christensen, J.; Tan, W.; Wilner, K. D.; Salgia, R.; Iafrate, A. J. Activity of crizotinib (PF02341066), a dual mesenchymal-epithelial transition (MET) and anaplastic lymphoma kinase (ALK) inhibitor, in a non-small cell lung cancer patient with de novo MET amplification. *J. Thorac. Oncol.* **2011**, *6*, 942−946.

(19) Chi, A. S.; Kwak, E. L.; Clark, J. W.; Wang, D. L.; Louis, D. N.; Iafrate, A. J.; Batchelor, T. Clinical improvement and rapid radiographic regression induced by a MET inhibitor in a patient with MET-amplified glioblastoma. Presented at ASCO 2011 Annual Meeting, Chicago, IL, June 3−7, 2011; Abstr. 2072.

(20) Lennerz, J. K.; Kwak, E. L.; Michael, M.; Fox, S. B.; Ackerman, A.; Bergethon, K.; Lauwers, G. Y.; Christensen, J. G.; Wilner, K. D.; Haber, D. A.; Salgia, R.; Bang, Y.; Clark, J. W.; Solomon, B. J.; Iafrate, A., J. Identification of a small and lethal subgroup of esophagogastric adenocarcinoma with evidence of responsiveness to crizotinib by MET amplification. Presented at ASCO 2011 Annual Meeting, Chicago, IL, June 3−7, 2011; Abstr. 4130.

(21) Munshi, N.; Jeay, S.; Li, Y.; Chen, C. R.; France, D. S.; Ashwell, M. A.; Hill, J.; Moussa, M. M.; Leggett, D. S.; Li, C. J. ARQ 197, a novel and selective inhibitor of the human c-Met receptor tyrosine kinase with antitumor activity. *Mol. Cancer Ther.* **2010**, *9*, 1544−1553.

(22) Sequist, L. V.; von Pawel, J.; Garmey, E. G.; Akerley, W. L.; Brugger, W.; Ferrari, D.; Chen, Y.; Costa, D. B.; Gerber, D. E.; Orlov, S.; Ramlau, R.; Arthur, S.; Gorbachevsky, I.; Schwartz, B.; Schiller, J. H. Randomized phase II study of erlotinib plus tivantinib versus erlotinib plus placebo in previously treated non-small-cell lung cancer. *J. Clin. Oncol.* **2011**, *29*, 3307−3315.

(23) Timofeevski, S. L.; McTigue, M. A.; Ryan, K.; Cui, J.; Zou, H. Y.; Zhu, J. X.; Chau, F.; Alton, G.; Karlicek, S.; Christensen, J. G.; Murray, B. W. Enzymatic characterization of c-MET receptor tyrosine kinase oncogenic mutants and kinetic studies with aminopyridine and triazolopyrazine inhibitors. *Biochemistry* **2009**, *48*, 5339−5349.

(24) Sun, L.; Liang, C.; Shirazian, S.; Zhou, Y.; Miller, T.; Cui, J.; Fukuda, J. Y.; Chu, J.-Y.; Nematalla, A.; Wang, X.; Chen, H.; Sistla, S.; Luu, T. L.; Tang, F.; Wei, J. Cho, Tang. Discovery of 5-[5-fluoro-2-oxo-1,2- dihydroindol-(3*Z*)-ylidenemethyl]-2,4- dimethyl-1*H*-pyrrole-3-carboxylic acid (2-diethylaminoethyl)amide, a novel tyrosine kinase inhibitor targeting vascular endothelial and platelet-derived growth factor receptor tyrosine kinase. *J. Med. Chem.* **2003**, *46*, 1116−1119.

(25) Bramson, H. N.; Corona, J.; Davis, S. T.; Dickerson, S. H.; Edelstein, M.; Frye, S. V.; Gampe, R. T., Jr.; Harris, P. A.; Hassell, A.; Holmes, W. D.; Hunter, R. N.; Lackey, K. E.; Lovejoy, B.; Luzzio, M. J.; Montana, V.; Rocque, W. J.; Rusnak, D.; Shewchuk, L.; Veal, J. M.; Walker, D. H.; Kuyper, L. F. Oxindole-based inhibitors of cyclin-dependent kinase 2 (CDK2): design, synthesis, enzymatic activities, and x-ray crystallographic analysis. *J. Med. Chem.* **2001**, *44*, 4339−4358.

(26) Christensen, J. G.; Schreck, R.; Burrows, J.; Kuruganti, P.; Chan, E.; Le, P.; Chen, J.; Wang, X.; Ruslim, L.; Blake, R.; Lipson, K. E.; Ramphal, J.; Do, S.; Cui, J. J.; Cherrington, J. M.; Mendel, D. B. A selective small molecule inhibitor of c-MET kinase inhibits c-MET-dependent phenotypes *in vitro* and exhibits cytoreductive antimutor activity *in vivo*. *Cancer Res.* **2003**, *63*, 7345−7355.

(27) PDB ID 2wkm for the PHA-665752/c-MET complex.

(28) Koenig, M.; Cui, J.; Wei, C. C.; Do, S. H.; Zhang, F.-J.; Vojkovsky, T.; Ramphal, J.; Yang, G.; Mattson, M.; Nelson, C.; Tang, P. C. Indolinone hydrazides as c-met inhibitors. PCT Int. Appl. WO2005005378, 2005.

(29) Vojkovsky, T.; Koenig, M.; Zhang, F.-J.; Cui, J. Tetracyclic compounds as c-Met inhibitors. PCT Int. Appl. WO2005004808, 2005.

(30) Zhang, F.-J.; Vojkovsky, T.; Huang, P.; Liang, C.; Do, S. H.; Koenig, M.; Cui, J. Preparation of triazolotriazines as c-Met modulators for treating cancer. PCT Int. Appl. WO2005010005, 2005.

(31) Cui, J.; Botrous, I. Arylmethyl triazolo and imidazopyrazines as c-MET inhibitors. PCT Int. Appl. WO2005004607, 2005.

(32) Zou, H. Y.; Li, Q.; Lee, J. H.; Arango, M. E.; Burgess, K.; Qiu, M.; Engstrom, L.; Yamazaki, S.; Parker, M.; Timofeevski, S.; Cui, J. J.; McTigue, M.; Los, M. G.; Bender, S.; Smeal, T.; Christensen, J. G. Sensitivity of Selected Human Tumor Models to PF-04217903, a Novel Selective c-Met Kinase Inhibitor. *Mol. Cancer Ther.* **2012**, *11*, 1036−1047.

(33) Yamazaki, S.; Skaptason, J.; Romero, D.; Vekich, S.; Jones, H. M.; Tan, W.; Wilner, K.; Koudriakova, T. Prediction of oral pharmacokinetics of cMet kinase inhibitors in humans: physiologi-cally-based pharmacokinetic modeling versus traditional one-compart-ment model. *Drug Metab. Dispos.* **2011**, *39*, 383−393.

(34) Trust, R. I.; Albright, J. D.; Lovell, F. M.; N. A. Perkinson, N. A. 6- and 7-aryl-1,2,4-triazolo[4,3-b]-1,2,4-triazines. Synthesis and characterization. *J. Heterocycl. Chem.* **1979**, *16*, 1393−1403.

(35) (a) Marusyk, A.; Vanessa Almendro, V.; Polyak, K. Intra-tumour heterogeneity: a looking glass for cancer? . *Nat. Rev. Cancer* **2012**, *12*, 323−334. (b) Szerlipa, N. J.; Pedrazab, A.; Chakravartyb, D.; Azimc, M.; McGuirec, J.; Fangd, Y.; Ozawae, T.; Hollande, E. C.; Hused, J. T.; Jhanward, S.; Levershac, M. A.; Mikkelseni, T.; Brennan, C. W. Intratumoral heterogeneity of receptor tyrosine kinases EGFR and PDGFRA amplification in glioblastoma defines subpopulations with distinct growth factor response. *Proc. Natl. Acad. Sci. U.S.A* **2012**, *109*, 3041−3046. (c) Gerlinger, M.; Rowan, A. J.; Horswell, S.; Larkin, J.; David Endesfelder, D.; Gronroos, E.; Martinez, P.; Matthews, N.; Stewart, A.; Tarpey, P.; Varela, I.; Phillimore, B.; Begum, S.; McDonald, N. Q.; Butler, A.; Jones, D.; Raine, K.; Latimer, C.; Santos, C. R.; Nohadani, M.; Eklund, A. C.; Spencer-Dene, B.; Clark, G; Pickering, L.; Stamp, G.; Gore, M.; Szallasi, Z.; Downward, J.; Futreal, P. A.; Swanton, C. Intratumor heterogeneity and branched evolution revealed by multiregion sequencing. *N. Engl. J. Med.* **2012**, *366*, 883−892.

(36) Zou, H. Y.; Li, Q.; Lee, J. H.; Arango, M. E.; McDonnell, S. R.; Yamazaki, S.; Tatiana B. Koudriakova, T. B.; Alton, G.; Cui, J. J.; Kung, P.-P.; Nambu, M. D.; Los, G.; Bender, B. L.; Mroczkowski, B.; Christensen, J. G. An orally available small-molecule inhibitor of c-Met, PF-2341066, exhibits cytoreductive antitumor efficacy through antiproliferative and antiangiogenic mechanisms. *Cancer Res.* **2007**, *67*, 4408−4417.